The Formation of Coherent Structures in the Context of Blocking

GEORG GOTTWALD AND ROGER GRIMSHAW

Department of Mathematics and Statistics, Monash University, Clayton, Victoria, Australia

(Manuscript received 28 April 1998, in final form 6 November 1998)

ABSTRACT

It is shown that the interaction of long, weakly nonlinear, quasigeostrophic baroclinic waves can be described by a pair of linearly coupled Korteweg–de Vries equations. Baroclinic energy conversion is investigated as the interaction of interacting upper- and lower-layer structures, which are represented by solitary waves. This system exhibits a rich dynamics that is suggestive of atmospheric blocking features, such as stable stationary solutions, transient quasi-steady-state solutions, multiple equilibria, and baroclinic instability. This system is investigated both analytically, using techniques from asymptotic perturbation theory, and through numerical simulations.

1. Introduction

Atmospheric blocking is the formation and development of quasi-stationary, highly persistent, and coherent high pressure fields in the midlatitude lower atmosphere. Present studies of blocking are concerned with the causes of their creation, maintenance, and decay. It is an important field of research because these atmospheric events are connected with anomalous weather situations and can have profound impact on midlatitude weather and climatic conditions, not only over the region in which they occur but over upstream and downstream areas as well. The duration of these events is also such that the timescale reaches the lower end of climatic timescales, leading to problems of long-range weather forecast and interannual variability.

The wealth of observational data and their diagnoses show that blocking involves both synoptic-scale and planetary-scale processes and their mutual interaction, that is, the interaction of baroclinic eddies with ultralong waves (Lupo and Smith 1995). The main mechanisms for the forcing and sustaining of a blocking high pressure system are still an open question and active field of research. There are mainly two competing points of view. One deals with resonant forcing by orography and addresses the question of multiple equilibria as stated for the first time by Charney and DeVore (1979). The other views blocking as a regional phenomenon forced by cyclones and baroclinic energy conversion (Hansen and Chen 1982). Simulations by Lindzen (1986) and Kalnay and Mo (1986) suggest that orography is not necessary for the formation and maintenance of a blocking system, but Egger et al. (1986) concede that, without any noneddy forcing, blocking systems would not have the observed amplitudes when friction is included, and, hence, we should take into account forcing by topography. In other words topography is not necessary to obtain blocking systems but does support its development. We will address this question and investigate the case of topographic forcing in a separate study.

As a starting point for investigating the problem of blocking systems, the quasigeostrophic potential vorticity equation is widely used. There are two main approaches. One deals with the full quasigeostrophic system and its numerical simulation, the other tries to simplify the system further into low-dimensional models. Numerical models integrating the barotropic potential vorticity equation are able to simulate anticyclonic blocking systems. These numerical experiments and also laboratory experiments (Linden et al. 1995) suggest that small-scale turbulent processes may be involved in the formation of blocking systems, although it should be noted that the experiments of Linden et al. (1995) were not performed in a meteorological context. To elaborate the physics of the turbulent nature of blocking, consider a nonrotating shallow fluid that is forced by sources and sinks. These sources and sinks can be viewed as representing sea surface temperature anomalies, mountains, etc., in an atmospheric model. It is well known that this approximately two-dimensional system exhibits an inverse energy cascade that will evolve into large-scale eddies. If rotation is added to the system, the two-dimensional character is reinforced according to the Taylor–Proudman theorem, but rotation can also introduce baroclinic instability. The latter is a three-dimensional feature and thus supports a direct en-

Corresponding author address: Dr. Georg Gottwald, INLN-CNRS, 1361 route des Lucioles, 06560 Valbonne Sophia-Antipolis, France. E-mail: gottwald@inln.cnrs.fr

ergy cascade toward small scales. Hence, the dynamics is determined by competing two-dimensional and three-dimensional processes (Metais et al. 1996; Bartello 1995; Bartello et al. 1996; Naulin 1995; Naulin et al. 1995). This picture fits into the work of Hansen and Sutera (1984), who compared the spectral transfer of energy and enstrophy during blocking and nonblocking situations and found a striking difference in the enstrophy transfer revealing a quasi-two-dimensional situation for the blocking case and a three-dimensional situation for the nonblocking case. A possible reason that we mainly observe anticyclones to be formed is due to the Čerenkov condition, which allows cyclones to decay through the radiation of linear Rossby waves if one takes into account divergent effects associated with the free surface (Nezlin 1994; Valcke and Verron 1996).

Whereas this picture represents an insightful and austere physical view into the general nature of anticyclonic blocking, it fails to provide analytical expressions and the infinite-dimensional character of a turbulent system has so far prevented a detailed analysis of more particular issues. One exception is the studies of modons, which are highly nonlinear solutions of the steady quasigeostrophic equations (Haines and Marshall 1987). In modon theory, potential vorticity is not a smooth function of the streamfunction but is multivalued corresponding to the interior and exterior regions. There is observational evidence (Ek and Swaters 1994) that this is the case for real blocking events. Nevertheless, this is a drawback for analytical progress. Therefore, interest has grown in low-dimensional models, although a rigorous proof of existence of a low-dimensional attractor in even quasigeostrophic systems is still an unsolved problem. The concept of a low-dimensional attractor was first introduced in meteorology by Lorenz (1980). Strictly speaking, one can only define a ''slowest invariant manifold'' (Bokhove and Shepherd 1996), since the small-scale events, that is, the high-frequency and high-wavenumber processes, enlarge the Hausdorff dimension for the attractor without any convergence (Yano and Mukougawa 1992). Thus the invariant set is often referred to as a ''fuzzy manifold'' (Warn and Menard 1986). This invariant set is of great importance for numerical weather prediction, because a projection of observed initial data on such a slowest, fuzzy manifold would allow data assimilation that eliminates high-frequency oscillations associated with free gravity waves triggered by insufficient initial data.

Numerical evidence of low-dimensional models exhibiting blocking systems was given by Legras and Ghil (1985). These low-dimensional models can be viewed as wave–wave interaction models. For an analytical treatment most work has utilized Galerkin approximations on the barotropic potential vorticity equation, that is, decomposing the pressure field into a Fourier series and truncating that series (Christensen and Wiin-Nielsen 1996). Nevertheless, low-order models have their drawbacks and have been critically reviewed, for example, in Tung and Rosenthal (1985) and Cehelsky and Tung (1985). It is argued there that multiple equilibria in low-order models might be an artifact of the truncation. A theoretical explanation was given by Yano and Mukougawa (1992) and addresses the nonexistence of a quasigeostrophic attractor, as mentioned above.

In order to bypass these drawbacks, to understand better the particular mechanisms involved in the formation of anticyclonic blocking, and to focus on the importance and impact of each, it is useful to look for a different simplification of the basic quasigeostrophic equations and study the derived model evolution equations. We will follow this latter track and perform a weakly nonlinear asymptotic analysis of the basic quasigeostrophic equations. Since blocking involves large-scale coherent structures, supposedly generated by baroclinic instability (Mullen 1987) and interacting with topography, we will introduce a model that supports coherent, localized solutions, namely, solitary waves, in an environment that can also support baroclinic instability and allows wave–wave interaction. We do not claim to be able to apply our asymptotic model directly to real blocking situations. Instead, our objective is to develop a self-consistent model that incorporates the main aspects of baroclinic instability relevant to blocking phenomena, in particular, the formation of coherent structures. Such models can provide insight into interpreting observations and numerical simulations.

To outline our weakly nonlinear approach we will briefly discuss the linear theory, on which most research concerning blocking systems has been based. The origins of the linear theory go back to the pioneering work of Charney (1947) and Eady (1949), who identified the fundamental physical process for baroclinic instability as the mutual intensification of two interacting Rossby waves. These waves propagate along waveguides consisting of high potential vorticity gradients. In modeling the atmosphere, we may relate these waveguides to the tropopause and surface, respectively, where gradients of potential vorticity are concentrated. Also, such specific properties as the upshear tilt with height of baroclinic unstable eddies can be explained within the framework of linear theory. The similarity between the fastest growing mode obtained by numerical simulation and the observed data is striking (Frederiksen 1992; Frederiksen and Bell 1990). In spite of these efforts, linear theory still fails to model baroclinic instability and blocking systems adequately in two important ways. First, there are the inherent disadvantages of linearization in general, such as unsaturated exponential growth, and the nonlocal structure of the solutions. Second, linear theory cannot explain features of blocking such as the observed decreased typical horizontal length scale and increased phase speed, when compared with linear simulations. The analysis of Dole (1982) of observations suggests an amplitude-dependent phase speed and, moreover, that the spatial scale of a blocking system is considerably larger and its propagation speed considerably smaller

than for typical baroclinic disturbances (Dole 1986). In particular, it is this latter point that leads us to believe that blocking can be modeled in the framework of solitary-wave dynamics.

Our approach is based on the pioneering work of Warn and Brasnett (1983), Patoine and Warn (1982), and Mitsudera (1994), who have extracted equations of the Korteweg–de Vries (KdV) type using a multiple-scale analysis. Whereas Warn and Brasnett (1983) and Patoine and Warn (1982) derived a single forced KdV equation for a wave in resonance with topography, Mitsudera (1994) investigated wave–wave interactions and hence derived a coupled system of two KdV equations. For completeness we shall also mention the works of Haines and Malanotte-Rizzoli (1991) and Malguzzi and Malanotte-Rizzoli (1984, 1985) who derived an unforced time-independent KdV equation and, hence, are not able to explain why blocks are observed to fluctuate in intensity during their life cycles and, even more, how they develop into a block. The question of a steady-state theory was also addressed by Helfrich and Pedlosky (1993, 1995) who derived a single Boussinesq equation. Their asymptotic analysis focuses on slightly subcritical zonal flows and neglects wave–wave interactions and, in comparison to our work, is therefore restricted to a smaller parameter range. We note that their single-wave equation can be derived from the coupled KdV equations in the asymptotic limit of slightly baroclinic unstable flows as was shown by Mitsudera (1994).

Our work stays close to that of Mitsudera (1994) and his time-dependent coupled KdV equations. His starting point is the continuous quasigeostrophic equation but he only took into account the first baroclinic mode. We will use a two-layer model bearing in mind that an N-layer model can only resolve the first N modes of a continuous model, for example, in the case of a two-layer model, the barotropic mode, and the first baroclinic mode. Mitsudera was interested in cyclogenesis, in particular, in cyclogenesis of type B where a large upper-level disturbance propagates into a low-level baroclinic zone and couples with a weak low-level anomaly. Therefore, he focused on the baroclinic unstable case and considered nonequilibrium solitary waves. To study blocking events we are more interested in coherent, quasistationary structures and therefore will mainly concentrate on equilibrium solutions of the coupled KdV equations. In this paper we will focus on the case when there is no topography. In a sequel we will examine the case of topographic forcing.

2. Quasigeostrophic two-layer model

Our principal aim here is to study baroclinic instability initiated by mode coupling in the weakly nonlinear, long-wave regime. For this purpose we choose the simplest model that can illustrate this process. Thus, we introduce a two-layer quasigeostrophic model on a β plane (Fig. 1). The upper layer is bounded above by a passive fluid with constant density ρ_0. This model can be used to represent either the atmosphere or the ocean. In the atmosphere the two layers model the troposphere and the stratosphere, respectively. In the ocean the density of the passive layer is set to zero. We also include frictional effects due to the presence of an Ekman layer at the lower boundary and a forcing effect due to topography, which is believed to be a crucial mechanism for the development of anticyclonic blocking systems, although a detailed discussion of the effect of topography is left for a sequel to this study.

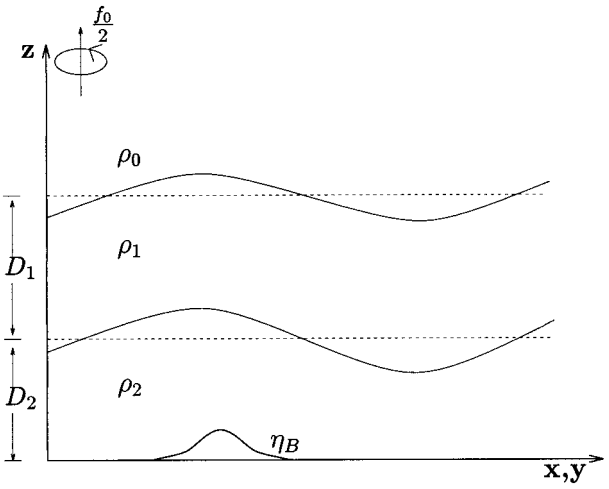

FIG. 1. Quasigeostrophic two-layer model.

We shall use a nondimensional coordinate system, based on a typical horizontal length scale L_0, typical vertical scales for each layer D_1, D_2 with $H_0 = D_1 + D_2$, and typical Coriolis parameter f_0. A typical velocity U is taken to be the maximum of the mean current velocity and the timescale is given by U/L_0. If we separate the mean flow U_1 and U_2 from the perturbation pressure fields p_1 and p_2, we obtain the following equations (Pedlosky 1987) for the nondimensional perturbation pressure fields:

$$\left(\frac{\partial}{\partial t} + U_n\frac{\partial}{\partial x}\right)q_n + \psi_{nx}Q_{ny} + J(\psi_n, q_n) = \begin{cases} 0 \\ -\dfrac{E_V^{1/2}}{2\epsilon}\Delta\psi_2, \end{cases} \tag{2.1}$$

where $n = 1, 2$, respectively, and

$$q_1 = \nabla^2\psi_1 + F_1(\psi_2 - \sigma_1\psi_1),$$

$$q_2 = \nabla^2\psi_2 - F_2(\psi_2 - \sigma_2\psi_1) + \eta_B, \tag{2.2}$$

$$Q_{1y} = \beta - U_{1yy} - F_1(U_2 - \sigma_1 U_1),$$

$$Q_{2y} = \beta - U_{2yy} + F_2(U_2 - \sigma_2 U_1), \tag{2.3}$$

with the Jacobian defined by $J(a, b) = a_x b_y - a_y b_x$. The boundary conditions are $\psi_{1,2} = \text{const}$ at $y = -L$,

0. Note that we adopt the usual convention that the frictional term in (2.1) acts only on the perturbation field; that is, an appropriate forcing term is added to the right-hand side of (2.1) to maintain the mean current.

Here the pressure fields are scaled by $\rho_{1,2} f_0 U_0 L_0$ and, in this quasigeostrophic approximation, also serve as streamfunctions for the velocity fields in each layer. The subscripts 1 and 2 are associated with the upper and lower layers, respectively. We have introduced the nondimensional meridional gradient of planetary vorticity β; the Rossby number $\epsilon = U/f_0 L_0$ ($\epsilon \ll 1$ in the quasigeostrophic approximation); the vertical Ekman number E_V, which is $O(\epsilon^2)$; $\sigma_1 = \rho_1(\rho_2 - \rho_0)/\rho_2(\rho_1 - \rho_0)$; $\sigma_2 = \rho_1/\rho_2$; $h_B = \epsilon D_2 \eta_B$, which is the nondimensional topography in the lower layer; and the Froude-numbers $F_n = (L_0/R_i)^2$, where R_i is the internal Rossby radius of deformation for each layer, that is, $R_i = f_0^{-1}\sqrt{gD_n(\rho_2 - \rho_1)/\rho_2}$. Note that $\sigma_1 > 1 > \sigma_2$ and usually we can use the Boussinesq approximation $\sigma_1 \approx \sigma_2 \approx 1$.

a. Linear model

Before we consider the weakly nonlinear, long-wave approximation, it is useful to discuss some properties of the linearized version of Eq. (2.1) in terms of a normal mode analysis (Pedlosky 1987). Here we shall restrict ourselves to the nondissipative and unforced case. Linearization of Eq. (2.1) yields

$$\left(\frac{\partial}{\partial t} + U_n \frac{\partial}{\partial x}\right) q_n + \frac{\partial \psi_n}{\partial x}\frac{\partial Q_n}{\partial y} = 0. \tag{2.4}$$

In terms of $\psi_n = \Re\{\Phi_n(y)\exp[ik(x - ct)]\}$ one obtains the necessary condition for baroclinic instability concerning the product of the meridional gradients of potential vorticity:

$$\left(\int_{-L}^{0} dy\, Q_{1y}\right)\left(\int_{-L}^{0} dy\, Q_{2y}\right) < 0. \tag{2.5}$$

It is this unstable region of exponentially growing modes for which a nonlinear model is primarily needed.

For the weakly nonlinear analysis to follow it is pertinent to note that when $F_1, F_2 \to 0$ (and also $\beta \to 0$), Eq. (2.4) decouples and has the linearly independent solutions $\Phi_n = A_n U_n$ with coincident phase speed $c = 0$ at $k^2 = 0$. Then a small perturbation in F_1, F_2, and β will generically open a gap in the linear spectrum in the stable case, or an unstable band in the unstable case (Craik 1985). The situation is sketched schematically in Fig. 2 where the phase speed c is plotted as a function of some generic system parameter Δ. Importantly, the nondegeneracy of the plots for c, and the linear independence of the two modes at the coalescence point, is the key reason why we eventually obtain *two* coupled equations when the system is perturbed. Since baroclinic instability in an inviscid context can only occur provided that there is such a mode resonance of two distinct

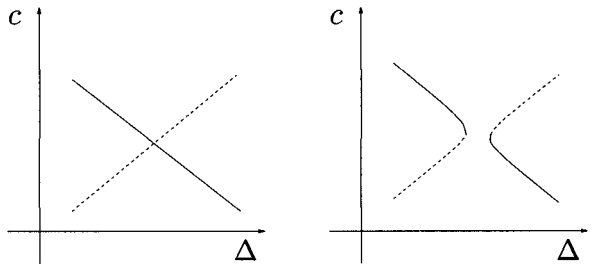

FIG. 2. Plots of phase speed c as a function of a system parameter Δ. (left) The case corresponding to the decoupled situation, i.e., $F_n = \beta = 0$; (right) corresponds to a perturbation on F_1, F_2, and β in the unstable case.

waves, it follows that in the long-wave limit we are apparently required to adopt this rather restrictive scaling of small F_i and β. In other words, the scaling is determined by the physical process under investigation. Note also that the coincident phase speed $c = 0$ also allows the system to be resonantly forced by topography. We state here again the difference of our work from that of Helfrich and Pedlosky (1993, 1995). They are elaborating their asymptotic expansion around the point of marginal instability of one branch in Fig. 2 and thus neglecting the gap, whereas we are also taking into account the interaction with the other mode and hence gain a much bigger parameter region for Δ. However, an advantage of their work is that there is no scaling of the equation parameters F_i and β involved.

b. Weakly nonlinear model

In the remainder of this section, we shall study weakly nonlinear long waves. We introduce the following scales:

$$X = \delta x, \quad T = \delta^3 t, \quad \psi_i = \delta^2 \psi_i^{(0)} + \delta^4 \psi_i^{(1)} + \cdots,$$
$$U_i = U_i^{(0)} + \delta^2 U_i^{(1)} + \cdots,$$

where δ is a small parameter, the inverse of which measures the horizontal scale of the disturbance. Next, we rescale the parameters

$$F_i \to \delta^2 F_i, \quad \beta \to \delta^2 \beta, \quad \eta_B \to \delta^4 \eta_B,$$
$$\frac{E_V^{1/2}}{2\epsilon} \to \delta^3 E. \tag{2.6}$$

The scaling of the Froude numbers was implied in section 2a. It follows that our model is valid for situations where the internal Rossby radius of deformation is of the order of the long horizontal scale. Further, the scaling of β implies that $Q_{iy} \approx -U_{iyy}$ at the lowest order. Since at this lowest order we require the linear decoupled system described in section 2a, we scale the bottom friction and the topography such that they contribute at the first nontrivial order. This scaling of the bottom friction means that the timescale for frictional damping is measured by the slow time T. Of course, from the point

of view of applications, if topography is present, then we are assuming it is in sympathy with these scales.

Substituting this scaling into Eq. (2.1), we obtain to the lowest order, $O(\delta^3)$,

$$U_i^{(0)}\psi_{iXyy}^{(0)} - U_{iyy}^{(0)}\psi_{iX}^{(0)} = 0,$$

from which we conclude that

$$\psi_i^{(0)}(X, T, y) = A_i(X, T)U_i^{(0)}(y). \tag{2.7}$$

Hence, the meridional structure of ψ_i is entirely determined by the mean currents at the leading order.

The $O(\delta^5)$ terms give us two evolution equations for the amplitudes A_i for each layer. We reiterate that the reason for the occurrence of two coupled equations is the scaling of the Froude numbers [(2.6)], which implies the existence of two independent modes at leading order. We obtain

$$U_i^{(0)}\psi_{iXyy}^{(1)} - U_{iyy}^{(0)}\psi_{iX}^{(1)} + G_i = 0, \tag{2.8}$$

where

$$\begin{aligned} G_1 = {} & A_{1T}U_{1yy}^{(0)} + U_1^{(0)}A_{1XXX}U_1^{(0)} \\ & + F_1U_1^{(0)}(U_2^{(0)}A_{2X} - \sigma_1U_1^{(0)}A_{1X}) + U_1^{(1)}A_{1X}U_{1yy}^{(0)} \\ & + A_{1X}U_1^{(0)}[\beta - U_{1yy}^{(1)} - F_1(U_2^{(0)} - \sigma_1U_1^{(0)})] \\ & + A_1A_{1X}(U_1^{(0)}U_{1yyy}^{(0)} - U_{1y}^{(0)}U_{1yy}^{(0)}), \end{aligned} \tag{2.9}$$

$$\begin{aligned} G_2 = {} & A_{2T}U_{2yy}^{(0)} + U_2^{(0)}A_{2XXX}U_2^{(0)} \\ & - F_2U_2^{(0)}(U_2^{(0)}A_{2X} - \sigma_2U_1^{(0)}A_{1X}) + U_2^{(1)}A_{2X}U_{2yy}^{(0)} \\ & + A_{2X}U_2^{(0)}[\beta - U_{2yy}^{(1)} + F_2(U_2^{(0)} - \sigma_2U_1^{(0)})] \\ & + A_2A_{2X}(U_2^{(0)}U_{2yyy}^{(0)} - U_{2y}^{(0)}U_{2yy}^{(0)}) + \gamma U_2^{(0)}\eta_{BX} \\ & + EA_2U_{2yy}^{(0)}. \end{aligned} \tag{2.10}$$

The solvability conditions are obtained by integrating (2.8) with respect to y so that, on using the boundary conditions, we get

$$\int_{-L}^{0} G_i\, dy = 0. \tag{2.11}$$

On substituting Eqs. (2.9) and (2.10) for G_i we obtain the amplitude equations for A_i:

$$A_{1T} + \Delta_1A_{1X} - \mu_1A_1A_{1X} - \lambda_1A_{1XXX} - \kappa_1A_{2X} = 0, \tag{2.12}$$

$$A_{2T} + \Delta_2A_{2X} - \mu_2A_2A_{2X} - \lambda_2A_{2XXX} - \kappa_2A_{1X} = D_X - EA_2, \tag{2.13}$$

where

$$\begin{aligned} I_n &= -[U_{ny}^{(0)}]_{-L}^{0}, \\ I_n\lambda_n &= \int_{-L}^{0} U_n^{(0)^2}\, dy, \\ I_n\mu_n &= -[U_{ny}^{(0)^2}]_{-L}^{0}, \\ I_1\Delta_1 &= -\int_{-L}^{0} (\beta - F_1U_2^{(0)})U_1^{(0)}\, dy - [U_1^{(1)}U_{1y}^{(0)}]_{-L}^{0}, \\ I_2\Delta_2 &= -\int_{-L}^{0} (\beta - \sigma_2F_2U_1^{(0)})U_2^{(0)}\, dy - [U_2^{(1)}U_{2y}^{(0)}]_{-L}^{0}, \\ I_1\kappa_1 &= F_1\int_{-L}^{0} U_1^{(0)}U_2^{(0)}\, dy, \\ I_2\kappa_2 &= \sigma_2F_2\int_{-L}^{0} U_1^{(0)}U_2^{(0)}\, dy, \\ I_2D &= \eta_B\int_{-L}^{0} U_2^{(0)}\, dy. \end{aligned} \tag{2.14}$$

Equations (2.12) and (2.13) have the form of two coupled KdV equations and, as expected, are similar to those derived by Mitsudera (1994). Note that for meridional symmetric and antisymmetric flows, or more generally just for $U_{iy}^{(0)} = 0$ at the boundaries, the nonlinear term vanishes. The coefficients μ_i determine the polarity of the solitary waves.

Before proceeding further, we shall rescale Eqs. (2.12) and (2.13) for convenience. We put

$$T \to \frac{T}{|\lambda_2|}, \qquad X \to (\text{sign}\lambda_2)X, \qquad A_n \to \frac{6\lambda_2}{\mu_2}A_n,$$

$$\Delta_n \to \lambda_2\Delta_n, \qquad \kappa_n \to \lambda_2\kappa_n, \qquad \mathcal{F} \to |\lambda_2|\mathcal{F},$$

$$D \to \lambda_2 D,$$

and

$$\mu = \frac{\mu_1}{\mu_2}, \qquad \lambda = \frac{\lambda_1}{\lambda_2},$$

in order to get

$$\begin{aligned} A_{1T} + \Delta_1A_{1X} - 6\mu A_1A_{1X} - \lambda A_{1XXX} - \kappa_1A_{2X} &= 0, \\ A_{2T} + \Delta_2A_{2X} - 6A_2A_{2X} - A_{2XXX} - \kappa_2A_{1X} &= D_X - EA_2. \end{aligned} \tag{2.15}$$

Next let us estimate the magnitude of the parameters of the system of coupled KdV equations (2.15). Since the parameters reflect the details of the mean flow structures, we need to use observational data, especially for the meridional gradients in both layers. We will estimate the order of the magnitude using a rough, but reasonable, approximation. We put $U_1 = \gamma U_2$, where $\gamma = D_2/D_1$, so that each layer has the same mass flux. This rough approximation yields

$$\mu \approx \gamma, \qquad \lambda \approx \gamma, \qquad \kappa_1 \approx F_1, \qquad \kappa_2 \approx \gamma\sigma_2 F_2.$$

If we choose $D_2 = 10$ km as the height of the troposphere and $D_1 = 2.5$ km as the height of the tropopause with densities $\rho_1 = 0.45$ kg m^{-3} and $\rho_2 = 0.85$ kg m^{-3}, and recall the typical synoptic scales as $L = 1000$ km, $U_0 = 10$ m s^{-1} and $f_0 = 10^{-4}$ s^{-1}, we obtain $\mu \approx \lambda \approx 4$, $\kappa_1 \approx 0.22$, and $\kappa_2 \approx 0.46$. Thus, realistic flow structures imply a weak coupling situation, which we will use later in a perturbation theory. Since the pressure fields ψ_i scale as $\rho f U_0 L$ and observed pressure fluctuations in synoptic systems are about 3×10^3 Pa, we find the amplitude A_i to be of the order of unity. In order to obtain numerical values for λ_2 and μ_2 needed for the scaling of the amplitudes we have used a mean flow structure, which is obtained by a trigonometrical least squares fit of the averaged, observed zonal flows at fixed seasonal times and at the 200-mbar surface (Oort and Rasmusson 1971; Gierling 1994), and again we have made the approximation of the same mass fluxes to obtain U_2. Since blocking systems are likely to occur during wintertime, the winter period was used only. The meridional mean flow gradients were evaluated in the midlatitudes at 45°.

c. Stability considerations

Before considering the full nonlinear problem, we will consider a linear stability analysis for Eq. (2.15). Thus, for the linearized, unforced equations, we put $A_i = A_{i0} \exp[ik(X - cT)]$ to obtain a quadratic equation for the phase velocity c, with the solutions

$$c_{1,2} = \frac{1}{2}(c_U + c_L) \pm \frac{1}{2}(\nu^2 + 4\kappa_1\kappa_2)^{1/2}, \quad (2.16)$$

where

$$c_U = \Delta_1 + \lambda k^2, \qquad c_L = \Delta_2 + k^2 - i\frac{1}{k}E,$$

$$\nu = c_U - c_L.$$

For $|\Delta_2 - \Delta_1| \to \infty$, that is, $\nu^2 + 4\kappa_1\kappa_2 \approx \nu^2$, we end up with two distinct modes c_U and c_L representing the decoupled phase velocities.

In the nondissipative case ($E = 0$) the criterion for instability is

$$(\Delta_2 - \Delta_1 + (1 - \lambda)k^2)^2 < -4\kappa_1\kappa_2, \quad (2.17)$$

which in the long-wave limit becomes

$$|\Delta_1 - \Delta_2| < 2\sqrt{-\kappa_1\kappa_2}. \quad (2.18)$$

The resulting necessary condition for instability

$$\kappa_1\kappa_2 < 0 \quad (2.19)$$

can be rewritten in terms of the mean flow gradients by using the definitions for κ_1 and κ_2 [(2.14)] as $I_1 I_2 < 0$. This is exactly a reduction of the condition for baroclinic instability [(2.5)] derived by linearizing the original quasigeostrophic two-layer system, for the present case when the shear flow is dominant compared to the β effect and there is weak coupling. According to (2.14) this implies $\lambda < 0$ since $I_i\lambda_i > 0$. Equation (2.18) puts a constraint on the velocity difference of the decoupled system in order that there be an instability.

The condition (2.19) can also be derived from the fully nonlinear system (with the omission of the forcing and dissipative terms) directly by multiplying the first equation of (2.15) with A_1 and the second equation with A_2 and integrating over the whole domain. After integration by parts, we obtain

$$\frac{1}{2}\frac{d}{dt}\int_{-\infty}^{+\infty} A_1^2\, dX = \kappa_1 \int_{-\infty}^{+\infty} A_1 A_{2X}\, dX$$

$$\frac{1}{2}\frac{d}{dt}\int_{-\infty}^{+\infty} A_2^2\, dX = -\kappa_2 \int_{-\infty}^{+\infty} A_1 A_{2X}\, dX, \quad (2.20)$$

and so

$$\frac{d}{dt}\left(\kappa_2 \int_{-\infty}^{+\infty} A_1^2\, dX + \kappa_1 \int_{-\infty}^{+\infty} A_2^2\, dX\right) = 0, \quad (2.21)$$

which immediately gives Eq. (2.19) as a necessary condition for baroclinic instability. Note that Eq. (2.17) could indicate linear stability in the long-wave limit ($k = 0$), but shorter waves may be linearly unstable. The dissipative case $E \neq 0$, which may involve a mode exchange, is discussed in appendix A.

d. Solitary waves

The KdV structure of Eq. (2.15) suggests that, in the absence of forcing and dissipation, there may be solitary-wave solutions. Since this system is not known to be integrable, we are not aware of any analytical techniques to construct such solutions. However, one explicit solution can be found of the following form:

$$A_i = a_i \operatorname{sech}^2[w(X - cT)]. \quad (2.22)$$

Substitution of this ansatz into (2.15) gives us the following relations for the parameters

$$c = \Delta_1 - 2\mu a_1 - \kappa_1\frac{\mu}{\lambda} = \Delta_2 - 2a_2 - \kappa_2\frac{\lambda}{\mu} \quad (2.23)$$

and

$$a_1 = 2\frac{\lambda}{\mu}w^2, \qquad a_2 = 2w^2, \quad (2.24)$$

so that $a_2/a_1 = \mu/\lambda$. Then elimination of the speed c gives the following necessary condition for the existence of this solitary wave:

$$\Delta_2 - \Delta_1 - 4(1 - \lambda)w^2 = \kappa_2\frac{\lambda}{\mu} - \kappa_1\frac{\mu}{\lambda}. \quad (2.25)$$

Note that Eq. (2.25) determines the allowed values for the coupling parameters κ_i and the linear phase veloc-

ities Δ_i needed to keep w_2 positive. Also given the system parameters (i.e., Δ_n, κ_n, μ, and λ) (2.25) determines a unique value of w and, hence, unique amplitudes a_n and speed c. Thus this solitary wave is apparently an isolated solution. Whether or not this is actually the case requires numerical simulations. We also note that Eq. (2.23) for the phase speed can be rewritten in the form

$$c^2 - c(\Gamma_1 + \Gamma_2) + \Gamma_1\Gamma_2 = \kappa_1\kappa_2, \qquad (2.26)$$

where

$$\Gamma_1 = \Delta_1 - 2\mu a_1 \quad \text{and} \quad \Gamma_2 = \Delta_2 - 2a_2. \qquad (2.27)$$

Further, the condition (2.25) for the equilibrium satisfying (2.24) can be rewritten in the form

$$\Gamma_2 - \Gamma_1 = \kappa_2\frac{\lambda}{\mu} - \kappa_1\frac{\mu}{\lambda}. \qquad (2.28)$$

Here, Γ_i are the speeds of a solitary wave in each decoupled KdV equation. Solutions of (2.26) for c yields exactly Eq. (2.16) for the linear phase velocity (with no dissipation, that is $E = 0$) provided that we replace the linear velocities Δ_i with the nonlinear velocities Γ_i. It follows that in the stable case ($\kappa_1\kappa_2 > 0$ and $\lambda > 0$) solitary waves of the form (2.22) can exist for all values of Γ_1, Γ_2 satisfying (2.28), while in the unstable case ($\kappa_1\kappa_2 < 0$ and $\lambda < 0$) the solitary waves exist only when $|\Gamma_2 - \Gamma_1| > 2\sqrt{-\kappa_1\kappa_2}$, that is, when the speed difference between the intrinsic solitary waves falls outside the linear instability band [cf. (2.18)]. We note that inhomogeneities of the mean flow can change the stability of the background since weak time dependencies enter only the coefficients Δ_i [see (2.14)]. Note that the equilibrium solution (2.28) is trivially outside of the range of baroclinic instability. Interestingly, it follows in both cases that these solitary waves can coexist with linear waves, in contrast to the general expectation that solitary waves occur only with speeds in the range of gaps in the linear spectrum.

We also note that the explicit analytical solution (2.22) is not necessarily the only one. Indeed, in section 3 we will construct approximate solutions by asymptotic methods.

Finally, we note here that Grimshaw and Malomed (1994) and Malomed et al. (1994) showed that for a linearly coupled KdV system such as (2.15) there is also another type of solitary wave, called gap solitons, which owe their existence to a gap in the frequency spectrum. We will not discuss this type of envelope solitary wave since one can easily show that they cannot exist in the parameter region defined by (2.14).

3. Asymptotic approximation

a. Introduction

For the analysis of the system of two coupled KdV equations (2.15) we will use both direct numerical simulations and an asymptotic approximation. In this approximation, the solitary-wave solutions of the KdV kernels of our system are used and it is assumed that the impact of small perturbations, that is, weak coupling, friction and topographic forcing, is essentially to modify the parameters of the unperturbed solitary waves on a slow timescale. Thus, we will model the full dynamics of the infinite-dimensional system by ordinary differential equations describing the evolution of the amplitudes and phases of each solitary wave. For a single KdV equation this method was first introduced by Johnson (1973) using a multiscale perturbation expansion, and later on using the inverse scattering technique by Karpman and Maslov (1978) and by Kaup and Newell (1978). An extension to this work was made by Grimshaw and Mitsudera (1993) using a multiscale perturbation expansion to take into account higher-order terms. We will follow this approach and will use the resulting amplitude and phase equations to extract information about solutions of the system of coupled KdV equations (2.15). In particular, we will rederive the steady-state conditions (2.23) and (2.25) and then, furthermore, discuss the stability properties of these steady states.

b. Asymptotic analysis

For our asymptotic analysis we introduce a small parameter $\epsilon \ll 1$ and assume that the perturbations κ_1, κ_2, E, and D are $O(\epsilon)$. As discussed above, the influence of these perturbations is to modify the amplitude and phase of the unperturbed KdV solitary waves (2.22) on a slow timescale of $O(\epsilon^{-1})$. A detailed description of the asymptotic development is given in appendix B. Here, we outline the main results. Thus, for the system of coupled KdV equations (2.15), we obtain at the leading order

$$u_0 = a_1(t)\,\mathrm{sech}^2[w_1(t)(x - \Phi_1(t))]$$
$$v_0 = a_2(t)\,\mathrm{sech}^2[w_2(t)(x - \Phi_2(t))] \qquad (3.1)$$

provided that

$$a_1 = 2\frac{\lambda}{\mu}w_1^2 \quad \text{and} \quad a_2 = 2w_2^2. \qquad (3.2)$$

The time evolution of the amplitudes a_i and phases Φ_i are determined by the following set of four ordinary differential equations:

$$\frac{da_1}{dt} = F_1(a_1, a_2, \Phi_1, \Phi_2),$$
$$\frac{da_2}{dt} = F_2(a_1, a_2, \Phi_1, \Phi_2),$$
$$\frac{d\Phi_1}{dt} = \Delta_1 - 2\mu a_1 + c_1^{(1)},$$
$$\frac{d\Phi_2}{dt} = \Delta_2 - 2a_2 + c_2^{(1)}, \qquad (3.3)$$

where the interaction integrals are given by

$$F_1 = -2\kappa_1 a_2 w_2 \int_{-\infty}^{\infty} \operatorname{sech}^2(\psi)\, \operatorname{sech}^2\left(\frac{w_2}{w_1}\psi - w_2\Delta\Phi\right) \tanh\left(\frac{w_2}{w_1}\psi - w_2\Delta\Phi\right) d\psi,$$

$$F_2 = -2\kappa_2 a_1 w_1 \int_{-\infty}^{\infty} \operatorname{sech}^2(\psi)\, \operatorname{sech}^2\left(\frac{w_1}{w_2}\psi + w_1\Delta\Phi\right) \tanh\left(\frac{w_1}{w_2}\psi + w_1\Delta\Phi\right) d\psi - \frac{4}{3}Ea_2$$
$$+ w_2 \int_{-\infty}^{\infty} \operatorname{sech}^2(w_2\psi) D_\psi(\psi + \Phi_2)\, d\psi, \tag{3.4}$$

and the first-order speed corrections by

$$c_1^{(1)} = -\kappa_1 \frac{\mu}{\lambda}\frac{w_2^3}{w_1^3} \int_{-\infty}^{\infty} \{\tanh(\psi) + \psi \operatorname{sech}^2(\psi) - \operatorname{sgn}(\lambda)\, \operatorname{tsanh}^2(\psi)\} \operatorname{sech}^2\left(\frac{w_2}{w_1}\psi - w_2\Delta\Phi\right) \tanh\left(\frac{w^2}{w_1}\psi - w_2\Delta\Phi\right) d\psi,$$

$$c_2^{(1)} = -\kappa_2 \frac{\lambda}{\mu}\frac{w_1^3}{w_2^3} \int_{-\infty}^{\infty} \{\tanh(\psi) + \psi \operatorname{sech}^2(\psi) - \tanh^2(\psi)\} \operatorname{sech}^2\left(\frac{w_1}{w_2}\psi + w_1\Delta\Phi\right) \tanh\left(\frac{w^1}{w_2}\psi + w_1\Delta\Phi\right) d\psi$$
$$+ \frac{1}{2a_2} \int_{-\infty}^{\infty} \{\tanh(w_2\psi) + w_2\psi \operatorname{sech}^2(w_2\psi) - \tanh^2(w_2\psi)\} D_\psi(\psi + \Phi_2)\, d\psi - \frac{E}{3w_2}. \tag{3.5}$$

The first-order speed corrections have contributions resulting from radiative tails, but they are only dynamically important for small amplitudes, as can be seen from (3.3). It is pertinent to mention that in the nontopographic, nondissipative case, neglecting these first-order speed corrections, Eq. (3.3) can be completely studied in the phase plane of $\Delta\Phi = \Phi_2 - \Phi_1$ and $\Delta A = 2\mu a_1 - 2a_2$.

Next, we note that from the system of coupled KdV equations (2.15) one can derive an energy equation, which was discussed in section 1c [see (2.21)] and is repeated here for convenience:

$$\frac{d}{dt}\int_{-\infty}^{\infty} \kappa_1 A_2^2 + \kappa_2 A_1^2\, dx = -2E \int_{-\infty}^{\infty} A_2^2\, dx + 2\int_{-\infty}^{\infty} A_2 D_x\, dx. \tag{3.6}$$

For the unforced ($D = 0$), nondissipative case ($E = 0$) the energy

$$\mathcal{E} = \int_{-\infty}^{\infty} \kappa_1 A_2^2 + \kappa_2 A_1^2\, dx$$

is conserved. Using the asymptotic expansion (3.1), we obtain at the lowest order that $\mathcal{E} = \mathcal{E}_0 + O(\epsilon)$, where

$$\mathcal{E}_0 = \frac{16}{3}\left(\kappa_2 \frac{\lambda^2}{\mu^2} w_1^3 + \kappa_1 w_2^3\right). \tag{3.7}$$

Indeed, it is readily verified that in the unforced, nondissipative case $\mathcal{E}_0$ is conserved by the amplitude equations (3.3) and, more generally, the full energy equation (3.6) is replicated in the amplitude equations (3.3). Thus topographic forcing can supply energy to the solitary waves. We also note that the frictional term can cause energy growth if $\mathcal{E} < 0$ (i.e., either or both of κ_1, $\kappa_2 < 0$), and thus instability may occur even when absent in the frictionless case.

For the nondissipative case there exists a conserved Hamiltonian for the full system of coupled KdV equations (2.15). Indeed, they can then be written as a noncanonical Hamiltonian system,

$$A_{1t} = -\partial_x \frac{1}{\kappa_2}\left(\frac{\delta\mathcal{H}}{\delta A_1}\right) \quad \text{and} \quad A_{2t} = -\partial_x \frac{1}{\kappa_1}\left(\frac{\delta\mathcal{H}}{\delta A_2}\right),$$

where δ denotes the functional derivative and $\mathcal{H}$ is the Hamiltonian density, which is found to be

$$\mathcal{H} = \kappa_2\left(\frac{1}{2}\Delta_1 A_1^2 - \mu A_1^3 + \frac{\lambda}{2}A_{1x}^2\right)$$
$$+ \kappa_1\left(\frac{1}{2}\Delta_2 A_2^2 - A_2^3 + \frac{1}{2}A_{2x}^2 - DA_2\right) - \kappa_1\kappa_2 A_1 A_2.$$

Due to the skew-symmetric operator ∂_x, the Hamiltonian $H = \int_{-\infty}^{\infty} \mathcal{H}\, dx$ is conserved.

If we now insert our ansatz (3.1) for A_1 and A_2 in the Hamiltonian H and calculate the leading-order term, we obtain the reduced Hamiltonian H_{red}:

$$H_{\rm red} = \kappa_2\left\{\frac{2}{3}\Delta_1\frac{a_1^2}{w_1} - \frac{4}{5}\mu\frac{a_1^3}{w_1}\right\} + \kappa_1\left\{\frac{2}{3}\Delta_2\frac{a_2^2}{w_2} - \frac{4}{5}\frac{a_2^3}{w_2}\right\} - \kappa_1\kappa_2 a_1 a_2\frac{1}{w_1}\int_{-\infty}^{\infty}\mathrm{sech}^2(z)\,\mathrm{sech}^2\left(\frac{w_2}{w_1}z - w_2\Delta\Phi\right)dz$$
$$- \kappa_1 a_2\int_{-\infty}^{\infty}\mathrm{sech}^2[w_2(z-\Phi_2)]D(z)\,dz. \tag{3.8}$$

After some lengthy algebra we can verify that $H_{\rm red}$ is conserved under the flow defined by the reduced system (3.3) provided that the nonadiabatic contribution of the radiative tails to the first-order speed corrections is omitted. It is pertinent to mention that only the reduced system including the first-order speed corrections, but omitting the radiative tail terms, is Hamiltonian and integrable.

c. Steady-state solutions

From this point on, we shall set the topographic forcing term $D = 0$. The important case when $D \neq 0$ will be discussed in a sequel to this paper. Further, since there are then only trivial equilibrium solutions if $E \neq 0$, we confine attention here to the nondissipative case $E = 0$. In this case there is then a nontrivial steady-state solution $a_1 = a_1^*$, $a_2 = a_2^*$, $\Phi_1 = \Phi_2 = ct$ with $w_1 = w_2 = w^*$. Note that then $\Delta\Phi = 0$, and the asymptotic system (3.3) is satisfied if

$$c = \Delta_1 - 2\mu a_1^* - \kappa_1\frac{\mu}{\lambda} = \Delta_2 - 2a_2^* - \kappa_2\frac{\lambda}{\mu}. \tag{3.9}$$

This is exactly the condition (2.23) found previously for the existence of an exact solitary wave solution of the full coupled KdV system (2.15). There may also be steady solutions of (3.3) with $w_1 \neq w_2$ but these cannot be exact solutions of the full coupled KdV system (2.15). These extraneous solutions can be analyzed using asymptotic methods or variational techniques (Gottwald 1998), but we shall not discuss them here any further.

We perform a linear stability analysis by linearization about this steady-state solution; that is, we write $\Phi_i = ct + \delta\varphi_i$ and $a_i = a_i^* + \delta a_i$. After some algebra we obtain

$$\delta\dot{a}_1 = \frac{8}{15}\kappa_1 a_2^{*2}\delta\Delta\varphi$$

$$\delta\dot{a}_2 = -\frac{8}{15}\kappa_2\frac{\mu}{\lambda}a_1^{*2}\delta\Delta\varphi$$

$$\delta\dot{\varphi}_1 = \left[-2\mu + \left(\frac{2}{3}+\frac{\pi^2}{45}\right)\kappa_1\frac{\mu}{\lambda}\frac{1}{a_1^*}\right]\delta a_1 - \left(\frac{2}{3}+\frac{\pi^2}{45}\right)\kappa_1\frac{1}{a_1^*}\delta a_2^* - \frac{8}{15}\,\mathrm{sgn}(\lambda)\kappa_1\frac{\mu}{\lambda}w^*\delta\Delta\varphi$$

$$\delta\dot{\varphi}_2 = \left[-2 + \left(\frac{2}{3}+\frac{\pi^2}{45}\right)\kappa_2\frac{\lambda}{\mu}\frac{1}{a_2^*}\right]\delta a_2 - \left(\frac{2}{3}+\frac{\pi^2}{45}\right)\kappa_2\frac{1}{a_2^*}\delta a_1 + \frac{8}{15}\kappa_2\frac{\lambda}{\mu}w^*\delta\Delta\varphi, \tag{3.10}$$

where the dot denotes the time derivative. We set δa_1, $= \delta a_1^{(0)}\exp(\gamma t)$, $\delta a_2 = \delta a_2^{(0)}\exp(\gamma t)$, etc., and obtain, omitting the superscripts, a system of linear equations:

$$\begin{pmatrix}0\\0\\0\\0\end{pmatrix} = \begin{pmatrix}-\gamma & 0 & -\xi & \xi\\ 0 & -\gamma & -\rho & \rho\\ \alpha & \beta & -\sigma-\gamma & \sigma\\ \epsilon & \eta & -\theta & \theta-\gamma\end{pmatrix}\begin{pmatrix}\delta a_1\\ \delta a_2\\ \delta\varphi_1\\ \delta\varphi_2\end{pmatrix}, \tag{3.11}$$

where the matrix elements are defined by (3.10). The solvability condition reads as

$$\gamma^2[\gamma^2 + (\sigma-\theta)\gamma + \xi(\alpha-\epsilon) + \rho(\beta-\eta)] = 0. \tag{3.12}$$

Two solutions are $\gamma = 0, 0$ and so the effective phase space is just two-dimensional. These trivial solutions $\gamma = 0$ correspond to the fact that, with $D = E = 0$, the nonlinear system can be reduced to three equations for a_1, a_2, and $\Delta\Phi$, and also then possesses the energy integral (3.7). To analyze the remaining roots of (3.12) we discuss some further simplifications.

It is pertinent to mention that we will talk here about instability not in the nonlinear sense of baroclinic instability as derived in Eq. (2.19) but in the sense of the solitary wave being a saddle point, which does not imply indefinite growth of the amplitudes as can be seen from (3.3). The reason for this is that the derived asymptotic equations (3.3) contain, besides equations for the amplitudes, also equations for the phase, that is, the location of the solitary wave. In the nonlinear criterion for instability we have integrated over the spatial scale and thus cannot obtain this kind of instability. The impact of the phase and position of the solitary wave on the stability will now be discussed.

1) No first-order speed corrections, no radiation

In this simplest case we can easily see that of all the parameters in (3.12) only α, η, ξ, and ρ are nonzero, so we obtain

$$\gamma^2 = \eta\rho - \alpha\xi = \frac{64}{15}w^4\left(\kappa^2\frac{\lambda}{\mu} + \kappa_1\mu\right) = \frac{16}{15}\kappa_1\mu\left(\frac{\kappa_2}{\kappa_1}\frac{1}{\lambda}a_1^{*2} + a_2^{*2}\right). \quad (3.13)$$

Hence, the fixed point can either be a saddle point, that is, $\gamma^2 > 0$, or a stable center, that is, $\gamma^2 < 0$. In this situation, the system, although not Hamiltonian, is time reversible and energy conserving. Recalling that the sign of λ is equal to the sign of $\kappa_1\kappa_2$ we find that the stability is entirely determined by the sign of $\kappa_1\mu$. In particular, the solitary wave is stable if $\kappa_1\mu < 0$ and unstable otherwise.

The physical significance of the sign of $\kappa_1\mu$ can be understood as follows. Let us assume, without loss of generality, an equilibrium state with $a_{1,2}^* > 0$ (i.e., $\lambda/\mu > 0$). If the solitary wave of the upper layer is displaced to the right, there will be a consequent change in amplitude and speed due to the forcing term $\kappa_1 A_{2x}$ associated with the lower-layer solitary wave. Since $A_{2x} = -2a_2 w\ \mathrm{sech}^2[w(x - ct)]\ \tanh[w(x - ct)]$ the sign of this forcing term is $-\mathrm{sgn}(\kappa_1)$ at the crest of the upper-layer solitary wave if displaced to the right and, hence, induces an amplitude change δa_1 whose sign is that of $-\mathrm{sgn}(\kappa_1)$ and whose consequent speed change δc has the opposite sign, namely, $\mathrm{sgn}(\kappa_1\mu)$, as can be easily seen from Eq. (3.9). But, in order for the equilibrium to be stable, the speed change δc should be negative so that the solitary wave can be restored to its equilibrium position. Thus stability requires $\kappa_1\mu < 0$. The same conclusion follows for a displacement to the left.

Note here that the Charney–Stern condition [(2.19)] for stability of the background state is not sufficient to ensure linear stability of this solitary-wave steady state. The reason for this is, as discussed above, that the criterion $\kappa_1\mu < 0$ is needed to ensure that the upper- and lower-layer solitary waves remain locked together and do not separate when subjected to small perturbations. We also note that the explosive instability found in the context of a Boussinesq equation by Helfrich and Pedlosky (1993) is already saturated in the coupled KdV system, which is equivalent to the Boussinesq equation in the limiting case of marginal stability as shown by Mitsudera (1994). In Helfrich and Pedlosky (1995) the authors show that the instability gets saturated in the full quasigeostrophic system.

2) First-order speed correction, but no radiation

If we include the first-order speed correction, we get two additional nonzero parameters, namely, ϵ and β, so that then

$$\gamma^2 = (\eta - \beta)\rho - (\alpha - \epsilon)\xi = \frac{16}{15}\kappa_1\mu\left(\frac{\kappa_2}{\kappa_1}\frac{1}{\lambda}a_1^{*2} + a_2^{*2}\right) - \frac{16}{15}\left(\frac{2}{3} + \frac{\pi^2}{45}\right)w^{*2}\left(\frac{\mu}{\lambda}\right)^2\left[\kappa_1 + \left(\frac{\lambda}{\mu}\right)^2\kappa_2\right]^2. \quad (3.14)$$

Since the second term is always negative, the contribution from the second-order speed correction is stabilizing. Equation (3.14) shows that this is enhanced, as discussed above, in the case of small amplitudes.

3) Radiation

In this general situation we obtain

$$\gamma = -\frac{\sigma - \theta}{2} \pm \sqrt{\frac{(\sigma - \theta)^2}{4} + \gamma_{\mathrm{nonrad}}^2}, \quad (3.15)$$

where γ_{nonrad} is determined either by (3.13) or by (3.14), depending on whether we exclude or include the first-order speed correction. Thus, since

$$\sigma - \theta = -\frac{8}{15}w\kappa_1\mu\left(\frac{1}{|\lambda|} + \frac{\kappa_2\lambda}{\kappa_1\mu^2}\right), \quad (3.16)$$

that is, $\mathrm{sgn}(\sigma - \theta) = -\mathrm{sgn}(\kappa_1\mu)$, a stable center ($\kappa_1\mu < 0$) is converted by radiation into a stable focus and a saddle point ($\kappa_1\mu > 0$) remains a saddle point but with enhanced growth rates.

4) Effect of friction

If we make the convenient assumption that the friction term is somehow balanced at the leading order, that is, we assume the existence of a nontrivial steady-state solution even in the presence of friction, the linearized system becomes

$$\delta\dot{a}_1 = \frac{8}{15}\kappa_1 a_2^{*2}\delta\Delta\varphi$$
$$\delta\dot{a}_2 = -\frac{8}{15}\kappa_2\frac{\mu}{\lambda}a_1^{*2}\delta\Delta\varphi - \frac{4}{3}E\delta a_2$$
$$\delta\dot{\Delta}\varphi = -2\delta a_2 + 2\mu\delta a_1, \quad (3.17)$$

where we have ignored the radiation and the first-order speed-correction terms. The equation for the growth rate γ is now

$$\gamma^3 + \frac{4}{3}E\gamma^2 - \frac{16}{15}\kappa_1\mu\left(a_2^{*2} + \frac{\kappa_2}{\kappa_1\lambda}a_1^{*2}\right)\gamma - \frac{64}{45}\kappa_1\mu a_2^{*2}E = 0. \quad (3.18)$$

Hence, for small friction a stable center is converted into a stable focus and a saddle point gains a third stable

manifold. However, this does not reflect the possible destabilizing effect of friction in a background environment where $\kappa_1\kappa_2 < 0$.

One can examine the solutions of (3.3) in general, looking in particular at the behavior of the amplitudes $a_{1,2}$ as $t \to \pm\infty$ on the orbits emanating from the saddle points. It is clear from (3.3) that if $\Delta\Phi \to \pm\infty$ in this limit, then the amplitudes $a_{1,2}$ approach well-defined stationary values, say, $a^{\pm}_{1,2}$. If the first-order speed-correction terms are included in the system (3.3) but the radiative terms are omitted so that the system conserves the Hamiltonian H_{red} of (3.8), then the system is integrable as it is third order (i.e., has only three effective variables a_1, a_2, and $\Delta\Phi$) and possesses two invariants, namely, ε_0 of (3.7) and H_{red} of (3.8). In this case the asymptotic values $a^{\pm}_{1,2}$ can, in principle, be determined explicitly in terms of $a^{*}_{1,2}$. This is achieved by equating the invariants $\mathcal{E}_0$ and H_{red} as $\Delta\Phi \to \pm\infty$ with the corresponding values at $\Delta\Phi = 0$. However, these algebraic relations are still quite complicated and can be evaluated only numerically. To achieve further detailed understanding one can consider the system (3.3) when further simplified by the omission of the first-order speed-correction terms altogether. But in this limit, the system is no longer Hamiltonian, and one must now resort to approximate methods to obtain expressions for $a^{\pm}_{1,2}$ (Gottwald 1998).

4. Numerical simulations of the coupled KdV system

In this section we will examine the dynamics of the system of the full coupled KdV equations (2.15) numerically, where here the topographic forcing term $D = 0$. Also, unless otherwise specified, the frictional term $E = 0$. To integrate this system a semi-implicit pseudospectral code is used, in which the linear terms are treated using a Crank–Nicholson scheme and the nonlinear terms using an explicit leapfrog scheme. Periodic boundary conditions are imposed in the x direction. To avoid self-interaction of the fields due to radiation tunneling through the periodic boundaries we introduce an artificial viscosity acting only near the boundaries.

In the following, we will simulate the behavior of the coupled KdV system with different parameter values and investigate the stability properties of the background and of possible coherent structures, that is, the steady-state solutions. First, however, we consider some typical mean flow structures [i.e., $U_{1,2}(y)$] that produce various parameter combinations. We recall that (2.14) determines the parameters while (2.17) and (3.13) determine the stability properties of the background and solitary-wave solution, respectively. To get an idea of typical mean flow structures resembling these parameter sets we have depicted some simple cases in Fig. 3. Note that Fig. 3c in particular is a mean flow configuration, which may be associated with blocking situations. It is pertinent to note that changing the sign of U_1 or U_2 changes

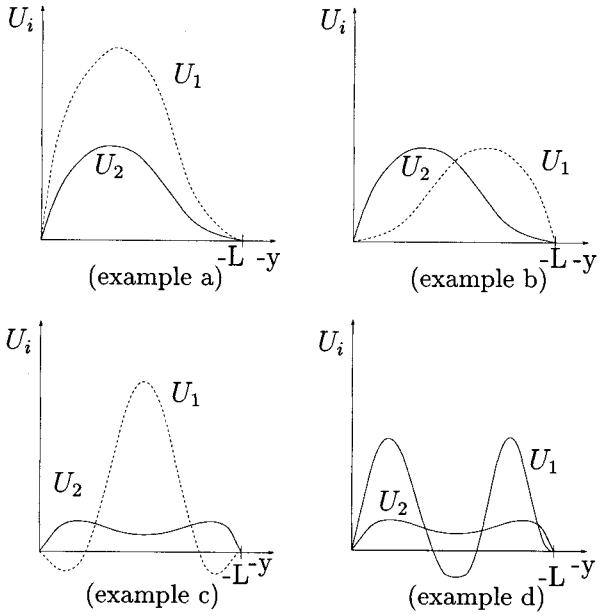

FIG. 3. Typical mean flow configurations. (a) (stable background, saddle point) $\kappa_1 > 0$, $\kappa_2 > 0$, $\mu > 0$, $\lambda > 0$; (b) (stable background, center) $\kappa_1 > 0$, $\kappa_2 > 0$, $\mu < 0$, $\lambda > 0$; (c) (stable background, saddle point) $\kappa_1 < 0$, $\kappa_2 > 0$, $\mu < 0$, $\lambda < 0$; (d) as in (a).

the signs of κ_2, μ, and λ, and thus changes the stability property of the corresponding steady-state solution, and of the background. If we wish to change the stability properties of the solitary wave without changing the background for a given mean flow configuration, we can simply switch the sign of μ by changing the sign of y in one layer without changing the signs of the other parameters [see (2.14)].

Although Eqs. (2.17) and (3.13) suggest the existence of an unstable solitary wave on an unstable background, it is important to mention that this scenario is not compatible with the underlying quasigeostrophic system, as readily seen from (2.25) and the implications of (2.14).

This section is organized to illustrate the several different scenarios of the rich dynamics of the coupled KdV system (2.15). First, we investigate the propagation of an upper-layer solitary-wave disturbance over a lower-layer background that is initially undisturbed. Second, we investigate the steady-state solutions found by the asymptotic theory. Third, we discuss solitary-wave interactions. As we will see the essential mechanism in each case is the interplay between the layers through the coupling terms, and the velocities of the solitary waves.

a. Basic solitary wave dynamics

The impact of an upper-layer solitary-wave disturbance on an undisturbed lower layer in a stable environment is to give birth to a secondary wave. Thus we suppose at $t = 0$, $A_2 = 0$ but A_1 has the typical KdV solitary-wave structure, that is, for instance, $A_1 = a_1$

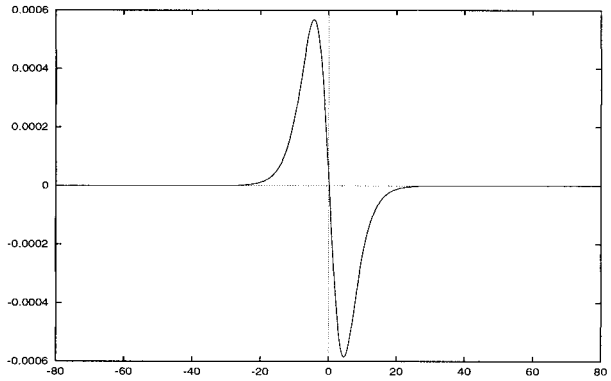

FIG. 4. Initial dipole in the lower layer triggered by an upper-layer solitary wave, where $\kappa_1 = 0.3$, $\kappa_2 = 0.1$, $\mu = -1$, $\lambda = -1$, $\Delta_1 = -1$, $\Delta_2 = 1$, and $a_1 = 0.05$.

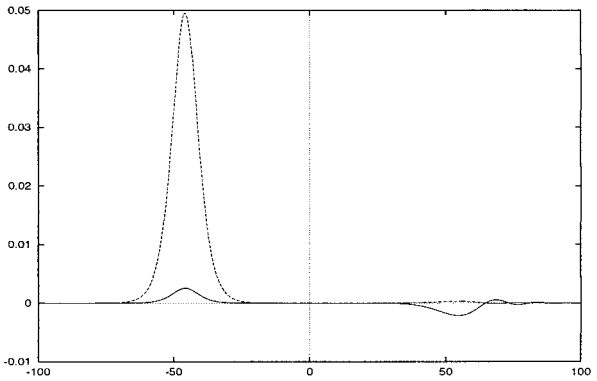

FIG. 5. Case of weak interaction; parameters as in Fig. 4 but for $t = 50$. The dashed line represents the upper-layer wave.

$\mathrm{sech}^2(w_1 x)$, with $a_1 = 2\lambda/\mu w_1^2$. Then at $t > 0$ it follows from (2.15) that $A_2 \approx \kappa_2 A_{1x} t$, which is the structure of the secondary wave at the time of creation. As shown in Fig. 4, initially this secondary wave has a dipole structure. Note that for $\kappa_2 < 0$ we would obtain the mirror image of Fig. 4. The further evolution of this dipole depends strongly on the difference between the phase velocity of the upper layer $v_1 = \Delta_1 - 2\mu a_1$ and the phase velocity of the lower layer $v_2 \approx \Delta_2$. If this difference is sufficiently high, the depression (or the elevation, depending on the direction of propagation of the upper-layer solitary wave) separates from the elevation (depression), escaping quickly enough to avoid interacting with the solitary wave, whereas the elevation (depression) will be captured by the upper-layer solitary wave and follow its motion. The escaping small-amplitude secondary wave being embedded in a stable background environment does not itself affect the dynamics of the upper-layer solitary wave and may decay after some time due to radiation (see Fig. 5). If, on the other hand, the difference of the phase velocities is small, the depression (elevation) cannot escape, and interacts with the solitary wave, generically leading to the formation of a locked state consisting of a generated secondary elevation (depression) in the upper layer and a depression (elevation) in the lower layer broadened by radiation. These locked states appear to be solitary-wave steady-state solutions that do not satisfy $w_1 = w_2$, as mentioned in section 3c. As in the previous case the elevation (depression) follows the motion of the upper-layer solitary wave, as can be seen in Fig. 6.

The slaved state of the secondary wave in the lower layer can be described by $A_1 = A_1(x - v_1 t)$ and $A_2 = A_2(x - v_1 t)$, where $v_1 = \Delta_1 - 2\mu a_1$, a_1 being the amplitude of A_1. If we neglect the nonlinear and the dispersive terms, the equation for the lower layer can be integrated to obtain an estimate for the ratio of the amplitudes. We find

$$A_2 = \frac{\kappa_2}{\Delta_2 - \Delta_1 + 2\mu a_1} A_1. \tag{4.1}$$

For the parameter values of Fig. 5 we calculate a ratio of 1:19 for the amplitudes, which fits with the numerically observed value up to an accuracy of 1.7%. We note that, although (4.1) implies $w_1 = w_2$, we expect that nonlinear and dispersive effects will lead to solutions with $w_1 \neq w_2$, as mentioned in section 3c.

The effect of friction is to dampen the dynamics. This causes the initially generated dipole to stay attached to the upper-layer disturbance. The dynamics of the lower layer is suppressed and therefore at each time only the forcing of the upper-layer solitary wave determines the dynamics of the lower layer leading to a slaved lower-layer dipole, which decreases in amplitude due to friction.

In the case of an unstable background environment the dynamics becomes more complex as can be seen in Fig. 7. The dominant dynamics can be filtered out if we look at the frictional case. The upper-layer disturbance grows due to the instability and emits a wave train moving upshear, which starts to grow baroclinically itself and, hence, interacts also significantly with the lower layer. It also generates a dispersive secondary wave train downshear in the lower layer by the mechanism discussed above. The higher the friction, the more the sec-

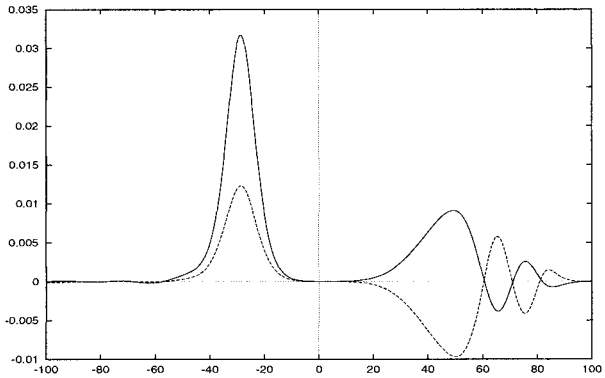

FIG. 6. Case of strong interaction; parameters as in Fig. 4 except $\Delta_1 = -0.1$, $\Delta_2 = 0.1$. The dashed line represents the lower-layer wave.

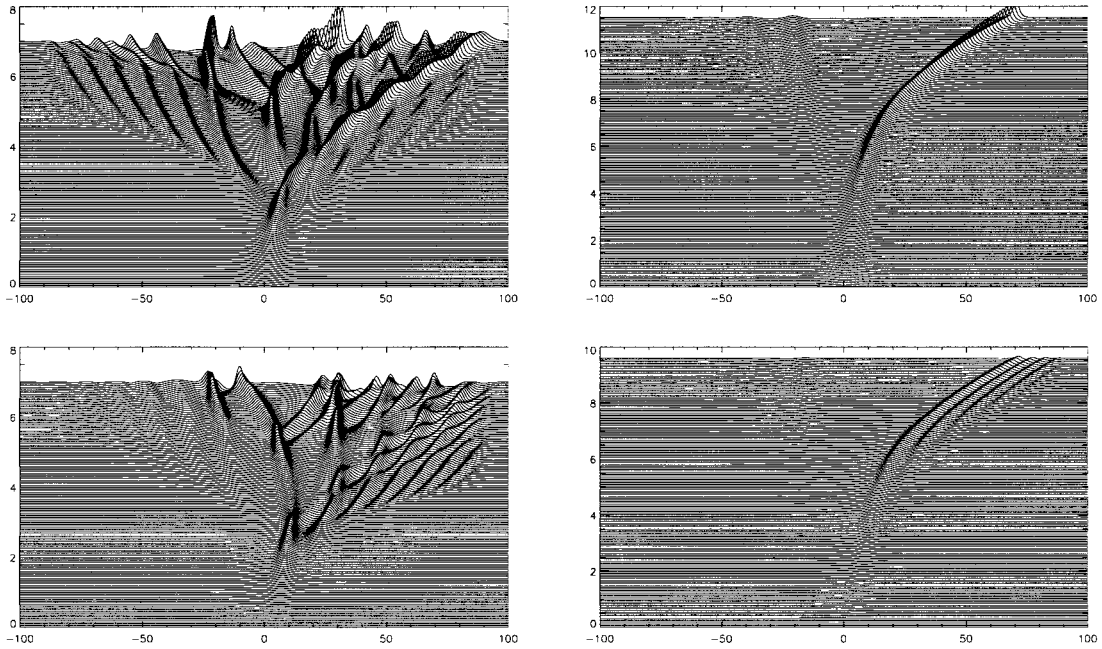

FIG. 7. Upper-layer solitary-wave disturbance on an unstable background with $\Delta_1 = 0$, $\Delta_2 = 0$, $\mu = -1$, $\lambda = -1$, $\kappa_1 = 0.3$, $\kappa_2 = -0.1$, and $a_1 = 0.05$. The left two plots refer to the nonfrictional situation; whereas for the right plots, friction is added with $E = 0.1$; the upper (lower) plots refer to the upper (lower) layer.

ondary wave stays phase locked to the upper-layer motion, and the less it disperses radiatively generated secondary wave trains. It is pertinent to mention that, although friction smoothes out the fields, it also may trigger instability on its own and thus gives rise to an increase of the upper-layer amplitudes and, hence, also of the lower-layer amplitudes [see (4.1) for instance]. This frictional instability has its origin in the possibility of negative energy and was discussed earlier in section 3b in our linear stability analysis.

b. Steady-state solutions

In a second set of simulations we will now investigate the properties of steady-state solutions, namely, the predictions of the asymptotic theory concerning the stability properties, which could be interpreted within that theory as saddle points or centers. The numerical simulation of the mean flow configuration, Fig. 3b, with the particular parameter values $\Delta_1 = -0.1$, $\Delta_2 = 0.1$, $\mu = -1.0$, $\lambda = 1.0$, $\kappa_1 = 0.3$, $\kappa_2 = 0.1$ and with the equilibrium solitary-wave amplitudes $a_1 = -0.6$ and $a_2 = 0.6$ (slightly disturbed), reveals the oscillatory nature of the center and reproduces the theoretical period $T = 16.03$ calculated using (3.13) with an accuracy of 0.5%. (The plots, not shown here, are qualitatively, similar to those of Fig. 15). If friction is added, the lower-layer solitary wave gets damped and the lower-layer dynamics is after some time completely determined by the forcing of the slowly decreasing upper-layer solitary wave and stays phase locked to it.

In an environment with $\kappa_1\kappa_2 < 0$, one can still obtain baroclinically stable solutions with appropriately chosen $\Delta_{1,2}$ according to (2.18) and again verify the predictions of the asymptotic theory. But in the frictional situation we may again observe frictional instability. The baroclinic instability induced by friction can be understood if we recall that a change in amplitude may put the solitary waves out of the stable band, as discussed in section 2d.

To study the dynamics of a saddle point we choose parameters referring to Fig. 3a or 3c, with $\kappa_1\kappa_2 > 0$. The existence of an unstable manifold amplifies numerical errors and, hence, the steady-state solution breaks up and the amplitudes approach the saturation value as $t \to \infty$ according to (3.3). The two perturbed waves interact in such a way, that they arrange to form a configuration revealing the upshear tilt with height, as shown in Fig. 8. In the frictional case the fields behave as discussed previously in the first set of numerical experiments for a stable environment; that is, they tend to form a phase-locked state with a forced dipole in the lower layer. It is important to emphasize that friction has the tendency to destroy the formation of an upshear-tilt-with-height configuration. This is apparent for this parameter values since $\kappa_2 > 0$ forces the field in the lower layer to look like the dipole depicted in Fig. 4.

c. Solitary wave interaction

In the next and last set of numerical simulations we look at solitary-wave interactions. We study the behav-

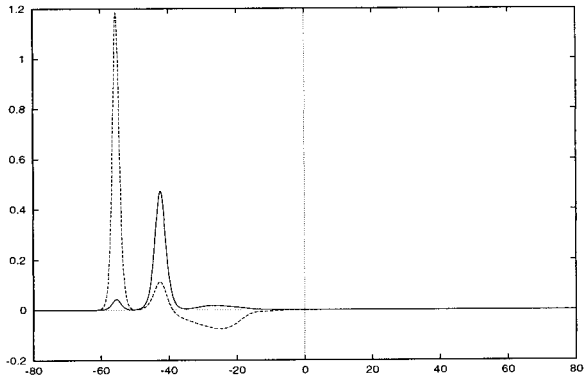

FIG. 8. Perturbed saddle point in a stable environment at time $t = 30$ with $\Delta_1 = 0.1$, $\Delta_2 = -0.1$, $\mu = \lambda = 1$, $\kappa_1 = 0.3$, and $\kappa_2 = 0.1$. The continuous line refers to the upper layer; the dashed line to the lower layer.

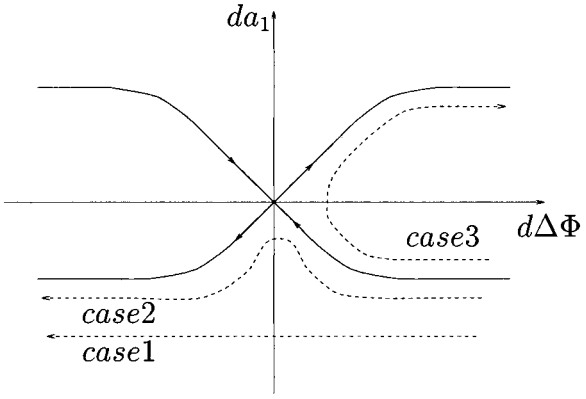

FIG. 9. Phase portrait of a saddle point with three generic scenarios.

ior of centers and saddle points in a stable environment. The possible scenarios for a saddle point can be studied in the da_1–$d\Delta\Phi$ plane of Fig. 9, which is qualitatively obtained from Eqs. (3.3) and (3.11). Here da_1 and $d\Delta\Phi$ represent the deviations from the steady-state values. There are three distinct scenarios depending on the initial conditions, namely, the regime of passage (case 1), the regime of quasi-locked states (case 2), and the regime of repulsion (case 3). Note that in the vicinity of the stable–unstable manifolds the system might switch from the locked regime to the repulsion, or vice versa due to slight perturbations. That means that the system under consideration allows the possibility of multiple states as discussed in Charney and DeVore (1979) even without topographical forcing but only through wave–wave interaction. In Figs. 10–12 numerical simulations corresponding to all three scenarios are shown.

The dynamics of the different regimes can be understood by means of the mutual generation of secondary waves. If the solitary waves run toward each other, each solitary wave will meet the secondary wave generated by the other layer and, hence, will increase (decrease) in amplitude. The manner and degree in which this increase (decrease) of the amplitudes affects the difference of the phase velocities $v_1 \equiv \Delta_1 - 2\mu a_1$ and $v_2 \equiv \Delta_2 - 2a_2$ determine the regime. If the impact is only marginal, the waves will propagate nearly undisturbed and maintain their direction of propagation. This corresponds to the passage regime as shown in Fig. 10. The interaction causes only emission of radiation in the direction of motion of each wave and generates a small wave extracted out of the main wave by the other wave. If the increase in amplitude is so large that v_1 and v_2 change their signs, we observe repulsion as in Fig. 11. If the interaction brings both velocities close to zero but does not alter the sign, we are faced with a quasi-locked state as in Fig. 12. In the context of blocking we would refer to this quasi-locked case 2 as a transient blocking system. According to the basic dynamics of the coupling as discussed earlier it is readily seen that the only parameter combination that allows the amplitudes of both layers to grow during interaction and hence support a sufficiently strong blocking system is $\mathrm{sgn}(\lambda) = \mathrm{sgn}(\mu) = \mathrm{sgn}(\kappa_1) = -1$ and $\mathrm{sgn}(\kappa_2) = +1$.

Let us now examine the impact of friction. In general, friction suppresses the generation of a secondary wave in the upper layer [see (4.1)] and of the small waves mentioned above and thus inhibits direct influence of the lower layer on the upper layer. In the passage regime and the repulsion regime the lower-layer wave decays and the dynamics of the lower layer is again, for sufficiently high friction, determined by the forcing of the upper layer. The frictional unstable situation, $\kappa_1\kappa_2 < 0$,

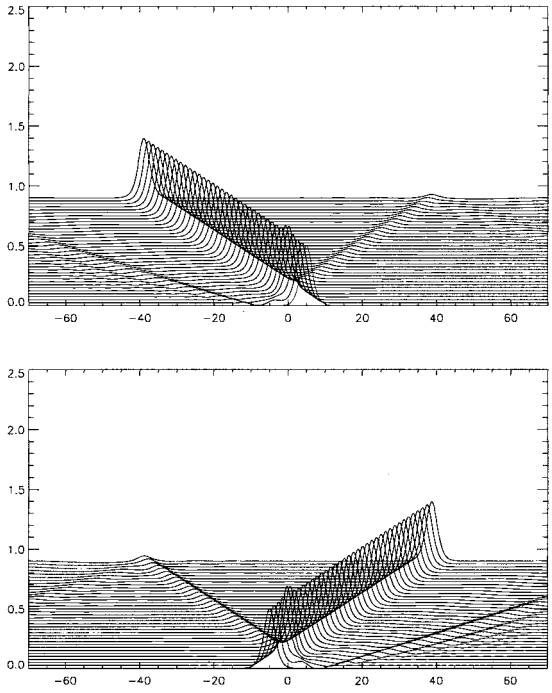

FIG. 10. Case 1: $\Delta_1 = -2.25$, $\Delta_2 = 2.25$, $\mu = \lambda = -1$, $\kappa_1 = -0.2$, $\kappa_2 = 0.3$, and $a_1 = a_2 = 0.5$.

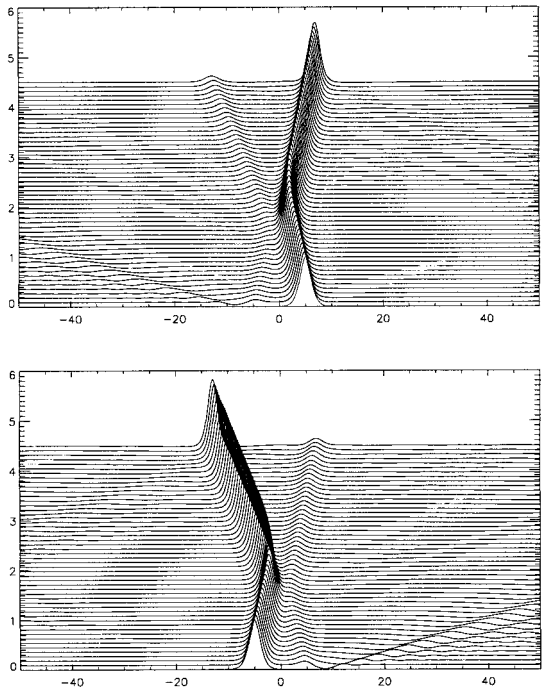

FIG. 11. Case 3: parameters as in Fig. 10 but $a_1 = a_2 = 1.0$.

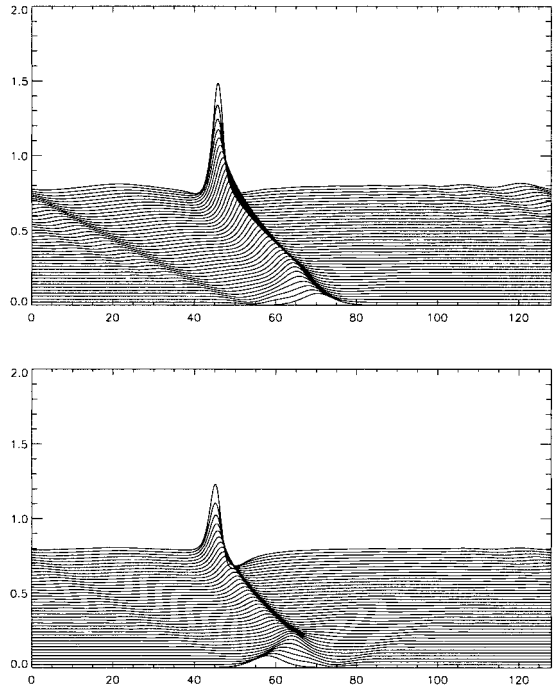

FIG. 13. Parameters as in Fig. 12 but with friction $E = 0.1$.

provides, as discussed above, the energy to increase the amplitudes. More drastically, the frictional instability can be observed in the locked state, where the two waves interact strongly. In Fig. 13 we show a numerical simulation at the same parameter values as in Fig. 12 but with $E = 0.1$. At smaller values of the friction an intermediate state is observed, where the wave splits into two parts: one is the slowly decaying original solitary wave keeping the direction of motion, the other is slaved by the upper layer. Thus, friction shuffles the energy from the original solitary wave into the slaved secondary wave. In the following evolution of these two solitary waves baroclinic instability is triggered. Thus, friction may provide a mechanism for the decay of a blocking system via triggering baroclinic instability.

To study the dynamics of two interacting stable centers we look at a corresponding generic phase portrait shown in Fig. 14. We find two regimes, namely, the regime of trapping inside the separatrix (case 1) and the

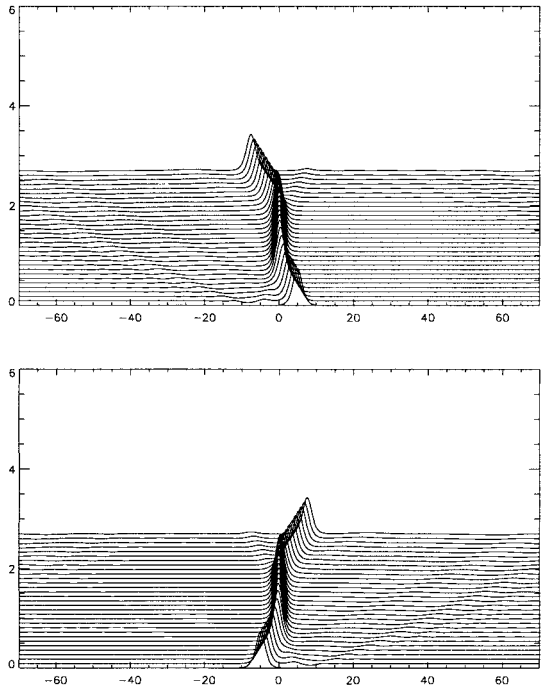

FIG. 12. Case 2: Parameters as in Fig. 10 but $a_1 = a_2 = 0.74$.

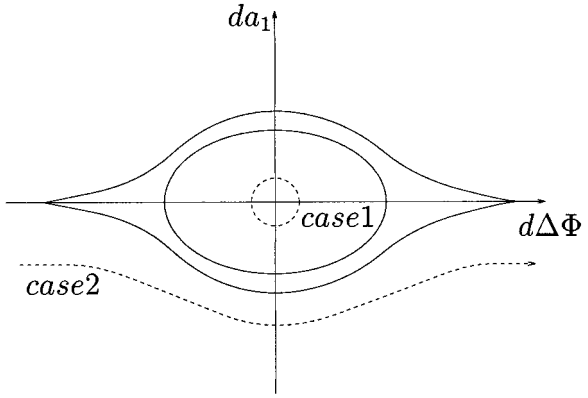

FIG. 14. Phase portrait of a stable center with two generic scenarios.

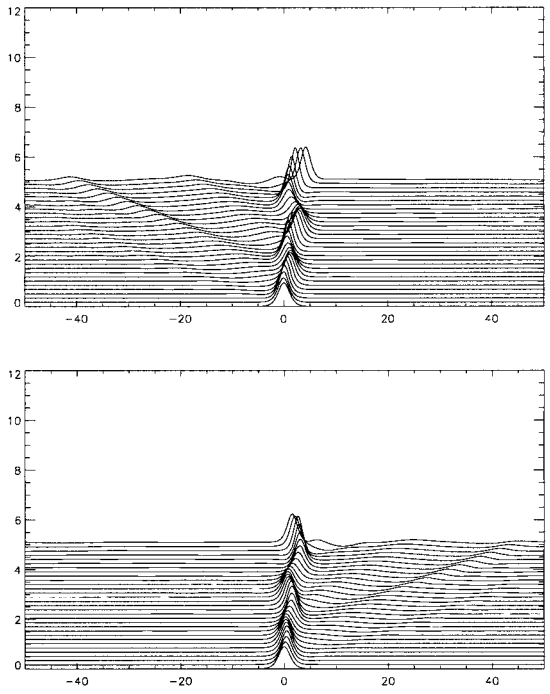

FIG. 15. Trapped regime for a stable center with $\Delta_1 = -1.7$, $\Delta_2 = 1.8$, $\mu = \lambda = -1$, $\kappa_1 = 0.3$, and $\kappa_2 = -0.2$, where the amplitudes of the solitary waves are $a_1 = 0.95$ and $a_2 = 0.9$.

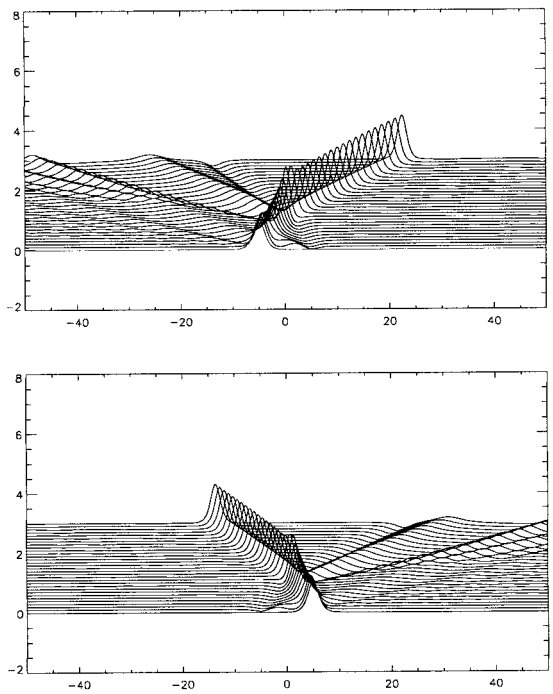

FIG. 16. Passage regime for a stable center for the same parameter values as in Fig. 15, where the solitary waves with $a_1 = a_2 = 1$ are dislocated initially by 10 spatial units.

regime of passage outside the separatrix (case 2). It turns out that the trapping regimes are hard to realize and are very sensitive to small disturbances revealing the local character of the asymptotic theory. Dislocations seem to destroy the regime more effectively than perturbations in the amplitudes. This is due to the strong interaction in the case of dislocations leading to secondary elevations and, hence, destroying the asymptotic regime. We will examine stable centers moving in a mean flow configuration such as Fig. 3a or 3c with a reversed upper-layer flow. Figure 15 shows mutually trapped solitary waves. The period of the oscillations in the amplitudes agrees with (3.13). This picture is obtained by a slight perturbation of the amplitudes. If we dislocate the initial solitary waves we force the solitons to change into the passage regime (see Fig. 16). The frictional case for these parameter values was already discussed above in the context of steady-state solutions revealing the fictional instability for $\kappa_1\kappa_2 < 0$. Again we observe the impact of friction as discussed above, such as slaving, suppression of direct interactions as the generation of secondary elevations, and frictional instability. Also, for stable centers, friction may provide a mechanism for the decay of coherent structures through baroclinic instability.

Strong interaction leading to the emission of dispersive wave trains can destroy the simple structure of the phase plane (Fig. 14). An example for such an interaction is shown in Fig. 17, where the initial waves are depressions. Although a direct theoretical explanation

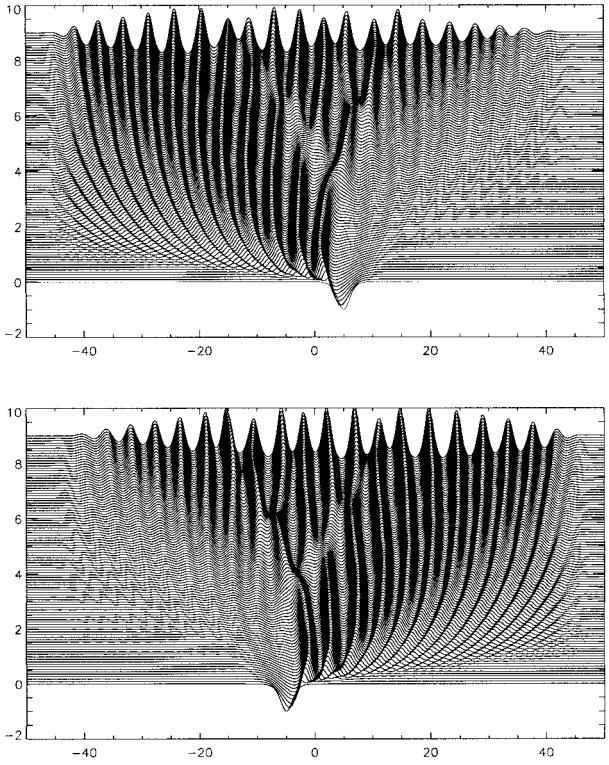

FIG. 17. Interacting stable centers with the parameter values $\Delta_1 = 2.25$, $\Delta_2 = -2.25$, $\mu = -1$, $\lambda = -1$, $\kappa_1 = 0.2$, $\kappa_2 = -0.3$, and $a_1 = a_2 = -1$.

using a phase plane is no longer possible, we try to explain this explosive scenario on a phenomenological base. Without loss of generality we restrict ourselves to the upper layer, recognizing the lower layer to be the mirror image of the upper layer. The elevations generated immediately by the lower layer tend to travel to the right since Δ_1 is bigger than zero. But the depression wave broadens into a background with negative amplitude, on which a solitary wave train then evolves. If we look at the equation for one of these solitary waves with amplitude a_1 traveling on a negative background d provided by the broadened center

$$a_{1T} + (\Delta_1 - 6\mu d)a_{1X} - 6\mu a_1 a_{1X} - \lambda a_{1XXX} - \kappa_1 A_{2X} = 0,$$

we readily conclude, that the impact of this background is to change the velocity. This explains the initial ''wrong'' direction of propagation for the elevations. The broader the depression becomes, that is, the smaller d gets, the less its influence becomes, and at later stages the elevations move according to the sign of Δ_1. The impact of friction on this process is to suppress the wave–wave interaction within each layer, and the generation of secondary wave trains by the the other layer on the upshear side.

5. Discussion and summary

Our purpose has been to present a theoretical basis for the formation and evolution of blocking systems in the atmosphere (or ocean). We have developed a weakly nonlinear long-wave theory describing the interaction of two long waves, as a reduction from a two-layer quasigeostrophic system. The dynamics of these waves was found to be described by a pair of coupled KdV equations. We believe that the solitary waves described here may be regarded as prototypes for coherent structures that can be observed in the atmosphere or ocean.

Investigating the validity and relevance of these solitary waves for the description of blocking systems and coherent structures has to be twofold. First, it has to be shown that the Korteweg–de Vries system (2.15) derived here is indeed a valid weakly nonlinear, long-wave approximation of the full quasigeostrophic two-layer system (2.1). We do so by numerically integrating the system (2.1) with the initial conditions being solutions of the coupled KdV equations (2.15), and testing how these solutions survive in the full quasigeostrophic system. Second, we have to examine whether the dynamics and predictions of the asymptotic theory are consistent with observations of real blocking events.

Here we give a preliminary account of some numerical simulations of the system (2.1). We used a finite-difference scheme, developed by Holland (1978). Here the problem is split into two parts; first we solve the Poisson equations for the barotropic mode $\Phi = \partial_t(F_2\psi_1 + F_1\psi_2)$ and the baroclinic mode $\Psi = \partial t(\psi_2 - \psi_1)$ where the inhomogeneous terms coming from the Jacobians are evaluated using the Arakawa scheme (Arakawa 1966). Then, in a second step, a second-order leapfrog scheme is used to determine the fields ψ_n where we take care of the time splitting by performing a forward time step after 75 time steps. Special attention has to be taken for the boundary conditions. On the walls of the channel we have $\partial\psi_n/\partial x = 0$. As discussed in Helfrich and Pedlosky (1995) this condition is empty for x-independent parts of ψ_n. With physical reasoning the condition can be modified to $\psi_n = 0$ at the channel walls for a localized pulse since we do not expect the perturbation field to be present in the far field. For periodic boundary conditions integrating (2.1) using the circulation theorem yields

$$\int \Psi \, dx \, dy = 0,$$

which is equivalent to imposing $\overline{\partial^2\psi_n/\partial t\partial x} = 0$ on the channel walls where the overbar denotes an x average. In the case of localized pulses we also implemented open boundaries using radiation conditions to avoid accumulation of Rossby waves at the eastern boundaries. We used an explicit Orlanski method (see, for instance, Han et al. 1983; Tang and Grimshaw 1996). Nevertheless, for some simulations it seemed to be more accurate to calculate the wave speeds exactly using the speeds of the fastest barotropic and baroclinic mode, rather than numerically using the Orlanski method.

For the mean flow, a profile of the form $U_i = U_{i0}(y - l_i)^2 \sin[\pi/L(y - y_{\max})]$ has been widely used where L is the channel width and U_{i0}, l_i are free parameters. The basic dynamics described in section 4a are beautifully reproduced in the numerical simulations of the full quasigeostrophic two-layer system, such as the formation of a dipole according to $A_2 \approx \kappa_2 A_{1x} t$. Moreover, the simulations can reproduce the results of our asymptotic perturbation theory. As an example we show in Fig. 18 a case where the first-order speed corrections stabilize according to (3.14) although $\kappa_1\mu > 0$. For the

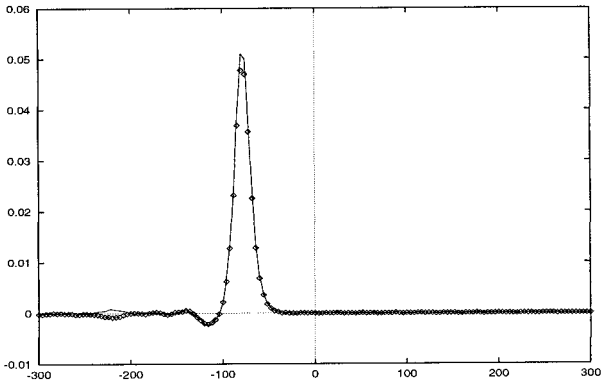

FIG. 18. Steady-state solution representing a center after $T = 100$. The continuous line refers to the upper layer, the dotted line to the lower layer.

mean flow we chose $U_{10} = 0.039$, $U_{20} = 0.01$, $L = 2$, $y_{max} = 1$, $l_1 = 9.0$, and $l_2 = 8.0$, and we set $\beta = 0.1$, $F_1 = 4.0$, $F_2 = 1.0$, and $\delta^2 = 0.15$, leading to $a_1^* = 0.15$, $a_2^* = 0.14$, $\lambda = 4.94$, $\mu = 4.39$, $\Delta_1 = 4.20$, $\Delta_2 = 5.13$, $\kappa_1 = 4.00$, $\kappa_2 = 4.93$, and for the time stretching according to the scaling to (2.6) $t = 84T$. In the x direction we used 350 grid points, in the y direction 10. Simulations investigating solitary-wave interactions will be presented in a sequel to this paper.

We will now briefly summarize and discuss the main features of the dynamics of the coupled Korteweg–de Vries equations (2.15) obtained by our asymptotic theory. In this asymptotic theory approximative solutions of the coupled KdV system could be found and stability criteria could be established, both for the background (a Charney–Stern condition for baroclinic instability) and also for the solitary wave solutions. The solitary waves could be interpreted as either centers or saddle points in a simplified phase-plane model. With respect to applications, centers may be identified with persistent blocking systems and the quasi-locked regime of the saddle points with transient blocking systems. The latter case is also interesting with respect to the theory of multiple equilibria since this quasi-locked state can be switched into a repulsion or passage regime by perturbation of the parameters involved (e.g., by changing the mean flow parameters). This can provide a mechanism for multiple states without the necessity for the inclusion of topography. For a critical review of the theory of multiple equilibria in low-order models, see Tung and Rosenthal (1985), Cehelsky and Tung (1985), and Yano and Mukougawa (1992).

We shall not attempt precise quantitative comparisons between our asymptotic theory and observed blocking events here, as our main purpose in this paper is to identify the possible dynamical scenarios. Further, it is more appropriate to consider detailed quantitative comparisons between observations and an appropriate set of numerical simulations of a full quasigeostrophic system. This aspect is currently under investigation and will be reported in detail elsewhere. However, we can point out here that the timescales and space scales of the dynamical scenarios found in our asymptotic theory are consistent with both observations (e.g., Dole 1983) and also full numerical simulations (e.g., Frederiksen 1997). Thus both observations and numerical simulations of the formation and development of mature blocking events show their lifetime to be around 10 days, and their pressure fields can increase up to three times within 5 days, before they reach their maximal pressure. In Fig. 19 we have depicted the amplitudes of the lower- and upper-layer solitary waves during an interaction of the quasi-locked type as depicted in Fig. 12. We see that the amplitudes increase during the course of interaction by a factor of 2, consistent with observations. The amplification of the pressure field in a quasi-blocked state from the premature block to a developed block can also be estimated using asymptotic theory (Gottwald 1998)

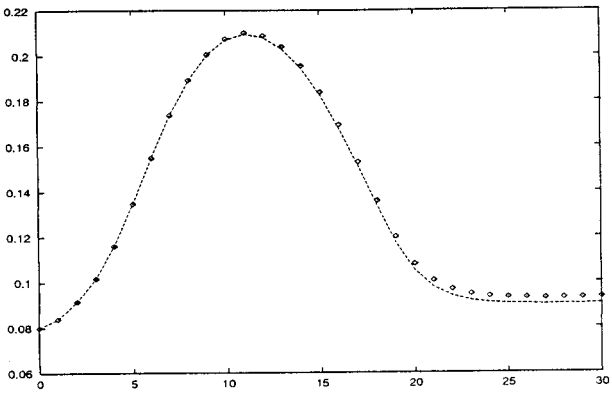

FIG. 19. Amplitudes of a quasi-locked state during the time of interaction. Parameters are $\Delta_1 = -1.5$, $\Delta_2 = 1.5$, $\mu = -1.0$, $\lambda = -1.0$, $\kappa_1 = -1.0$, and $\kappa_2 = 1.0$. The continuous line refers to the upper layer, the dotted line to the lower layer.

and is also in good agreement with observations. The timescale of a quasi-locked blocking event can be estimated using Fig. 19 if we assume a typical horizontal length-scale 1000 km, a typical velocity of the meanflow 10 m s^{-1}, set the governing small parameter of the long-wave theory $\delta = 0.5$, and let $|\lambda_2|$ be of $O(1)$. We obtain lifetimes for the quasi-locked blocking systems greater than 10 days. The reason for the overestimation of blocking times might be that in a long-wave approximation small-scale effects that tend to weaken the system are filtered out.

For the decay of blocking systems, friction was identified as a possible mechanism for triggering baroclinic instability in both the quasi-locked states and in the stable steady-state solutions. Furthermore, inhomogeneities in the mean flow provide another mechanism in our model to trigger baroclinic instability as discussed in section 2d. The destruction of mature blocking systems through baroclinic instability has been found in observations and has been discussed by Dole (1986) and Lupo and Smith (1995).

To summarize, we see that our weakly nonlinear, long-wave analysis of the quasigeostrophic two-layer model, and the derived coupled Korteweg–de Vries equations are highly suggestive of blocking systems. In a sequel to this paper we will report further on the case when topographic forcing is present, using asymptotic methods analogous to those used here, and also on solitary-wave interactions using numerical simulations of the full quasigeostrophic two-layer system.

Acknowledgments. We gratefully acknowledge the support of the Deutscher Akademischer Austauschdienst, which sponsored this work through the HSP II/AUFE; of the CRC–Southern Hemisphere Meteorology; and ARC Grant A89600523.

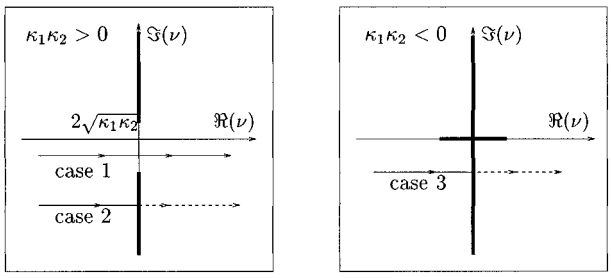

FIG. A1. Loci of ν on the upper Riemann surface as $(\Delta_2 - \Delta_1)$ varies. Bold lines are branch cuts where $\sqrt{\nu^2 - 4\kappa_1\kappa_2}$ is real. The dashed line indicates the passing from the upper Riemann surface onto the lower one.

APPENDIX A

Linear Stability for $E \neq 0$

To investigate the linear stability in the dissipative case we will consider the long-wave limit ($k \to 0$) and examine the Riemann surface in the $\Re(\nu)$–$\Im(\nu)$-plane; the $\Re(\sqrt{\nu^2 + 4\kappa_1\kappa_2}) = 0$ branches are shown in Fig. A1. Note that the $\Im(\nu) = 0$ branch cut is redundant since it implies $E = 0$. If we define the upper Riemann surface by $\Re(\sqrt{\nu^2 + 4\kappa_1\kappa_2}) > 0$, there are typically two cases in the behavior of ν as $\Delta_2 - \Delta_1$ varies, as shown in Fig. A1. Without loss of generality we put $\Re(\sqrt{\nu^2 + 4\kappa_1\kappa_2}) > 0$ as $\Delta_2 - \Delta_1 \to \infty$; then, in case 1, ν remains on the upper Riemann surface, whereas in case 2 and case 3 it passes onto the lower Reimann surface $\Re(\sqrt{\nu^2 + 4\kappa_1\kappa_2}) < 0$. Since $\Re(\nu)$ is negative (positive) as $(\Delta_2 - \Delta_1) \to \infty$ $(-\infty)$, we obtain

$$\sqrt{\nu^2 + 4\kappa_1\kappa_2} \sim \begin{cases} -\nu & \text{as } \Delta_2 - \Delta_1 \to \infty \\ \begin{cases} \nu & \text{(case 1)} \\ -\nu & \text{(case 2, case 3).} \end{cases} & \text{as } \Delta_2 - \Delta_1 \to -\infty. \end{cases}$$

Thus, in case 1 an exchange of the modes c_U, c_L occurs in the vicinity of $\Re(\nu) = 0$, while there is no such exchange in cases 2 and 3. Note that $\Re(\nu) = 0$ refers to the equality of the phase speeds of the decoupled system. The growth rate becomes in the vicinity of $\Re(\nu) = 0$ for $\kappa_1\kappa_2 > 0$,

$$\Im(c) = -\frac{1}{2k}E \quad \text{(case 1)}$$

$$= -\frac{1}{2k}E \pm \frac{1}{2k}\sqrt{E^2 - 4\kappa_1\kappa_2} \quad \text{(case 2),} \quad \text{(A1)}$$

and for $\kappa_1\kappa_2 < 0$,

$$\Im(c) = -\frac{1}{2k}E \pm \frac{1}{2k}\sqrt{E^2 - 4\kappa_1\kappa_2} \quad \text{(case 3).} \quad \text{(A2)}$$

Thus, for $\kappa_1\kappa_2 > 0$, $\Im(c)$ is always negative in both cases; but for $\kappa_1\kappa_2 < 0$ there is always an exponentially amplifying part. Typical situations are depicted in Fig. A2 and Fig. A3.

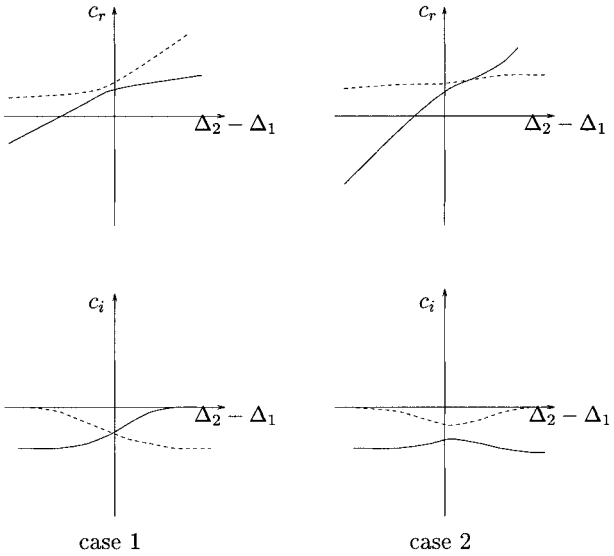

FIG. A2. Typical linear dispersion curves for $\kappa_1\kappa_2 > 0$.

APPENDIX B

Detailed Asymptotic Analysis

We recall the system of coupled KdV equations (2.15):

$$A_{1t} + \Delta_1 A_{1x} - 6\mu A_1 A_{1x} - \lambda A_{1xxx} - \epsilon\kappa_1 A_{2x} = 0,$$
$$A_{2t} + \Delta_2 A_{2x} - 6A_2 A_{2x} - A_{2xxx} + \epsilon(-\kappa_2 A_{1x} - D_x + EA_2) = 0, \quad \text{(B1)}$$

where, for convenience, we have introduced a small parameter $\epsilon \ll 1$ and have assumed that κ_1, κ_2, E, and D are $O(\epsilon)$. We also introduce the slow timescale $T = \epsilon t$, on which the amplitudes and phases are assumed to

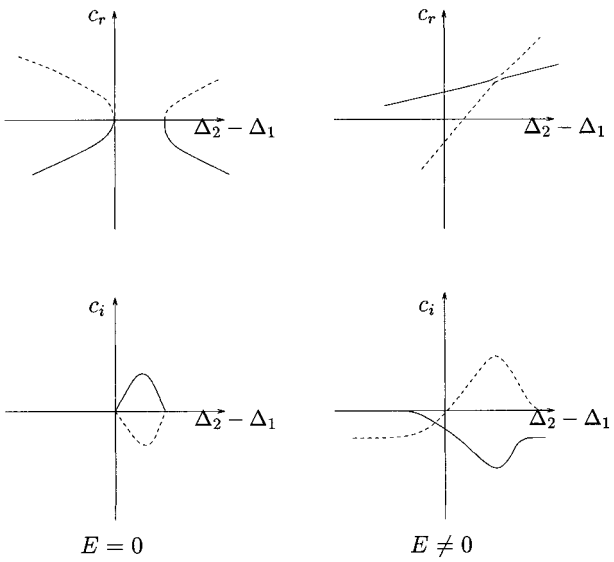

FIG. A3. Typical linear dispersion curves for $\kappa_1\kappa_2 < 0$.

evolve. Later on, we will restore the original parameters back into the final system of ordinary differential equations.

For our asymptotic analysis we seek an asymptotic expansion of the form

$$\begin{aligned} A_1 &= u_0 + \epsilon u_1 + \epsilon^2 u_2 + \cdots \\ A_2 &= v_0 + \epsilon v_1 + \epsilon^2 v_2 + \cdots \\ u_0 &= a_1(T)\,\mathrm{sech}^2\{w_1(T)[x - \Phi_1(T)]\} \\ v_0 &= a_2(T)\,\mathrm{sech}^2\{w_2(T)[x - \Phi_2(T)]\} \\ \Phi_i &= \frac{1}{\epsilon}\int_0^T c_i(T')\,dT' \qquad i = 1, 2 \\ c_i &= c_i^{(0)} + \epsilon c_i^{(1)} + \cdots \qquad i = 1, 2. \end{aligned} \tag{B2}$$

Substitution of these expansions into the Eq. (B1) yields, at the leading order,

$$\begin{aligned} (\Delta_1 - c_1^{(0)})u_{0x} - 6\mu u_0 u_{0x} - \lambda u_{0xxx} &= 0 \\ (\Delta_2 - c_2^{(0)})v_{0x} - 6v_0 v_{0x} - v_{0xxx} &= 0, \end{aligned} \tag{B3}$$

which is solved by our ansatz (B2) for u_0 and v_0, provided that

$$\begin{aligned} a_1 &= 2\frac{\lambda}{\mu}w_1^2, \qquad a_2 = 2w_2^2 \quad \text{and} \\ c_1^{(0)} &= \Delta_1 - 2\mu a_1, \qquad c_2^{(0)} = \Delta_2 - 2a_2. \end{aligned} \tag{B4}$$

Of course, these are just the well-known solitary-wave solutions of the KdV equations obtained by setting $\epsilon = 0$ in (B1).

We introduce the following two linear operators:

$$\begin{aligned} H_1 &= -\lambda\partial_{xx} - 6\mu u_0 - (c_1^{(0)} - \Delta_1) \\ H_2 &= -\partial_{xx} - 6v_0 - (c_2^{(0)} - \Delta_2). \end{aligned} \tag{B5}$$

Note that $H_{1,2}$ are self-adjoint and that, at the leading order, Eq. (B3) becomes

$$H_1 u_{0x} = 0, \qquad H_2 v_{0x} = 0. \tag{B6}$$

At the next order, $O(\epsilon)$, we obtain a linear equation for u_1 in the upper layer:

$$\begin{aligned} &(\Delta_1 - c_1^{(0)})u_{1x} - 6\mu\partial_x(u_0 u_1) - \lambda u_{1xxx} \\ &\quad = c_1^{(1)}u_{0x} + \kappa_0 v_{0x} - u_{0T}. \end{aligned} \tag{B7}$$

To obtain the solvability condition for this equation we investigate the related adjoint homogeneous equation, which is

$$H_{1\varphi x} = 0.$$

Besides the trivial solution $\phi = 1$, this has the linearly independent solutions $\phi = u_0$ and

$$\begin{aligned} \varphi_x = \theta_1\,\mathrm{sech}^2(\theta_1)\tanh(\theta_1) + \frac{2}{15}\cosh^2(\theta_1) + \frac{1}{3} \\ - \mathrm{sech}^2(\theta_1), \end{aligned} \tag{B8}$$

where $\theta_1 = w_1(x - \Phi_1)$. Since this solution is unbounded as $\theta_1 \to \pm\infty$, the solvability condition is just

$$\int_{-\infty}^{\infty}(c_1^{(1)}u_{0x} + \kappa_1 v_{0x} - u_{0T})u_0\,d\theta_1 = 0. \tag{B9}$$

Substitution of u_0 and v_0 gives us the desired evolution equation for the amplitude a_1:

$$\frac{da_1}{dt} = -2\kappa_1 a_2 w_2 \int_{-\infty}^{\infty}\mathrm{sech}^2(\theta_1)\,\mathrm{sech}^2\left(\frac{w^2}{w_1}\theta_1 - w_2\Delta\Phi\right)\tanh\left(\frac{w_2}{w_1}\theta_1 - w_2\Delta\Phi\right)d\theta_1, \tag{B10}$$

where $\Delta\Phi = \Phi_2 - \Phi_1$. In the lower layer we get at the order, $O(\epsilon)$, the following linear equation for v_1:

$$\begin{aligned} &(\Delta_2 - c_2^{(0)})v_{1x} - 6\partial_x(v_0 v_1) - v_{1xxx} \\ &\quad = c_2^{(1)}v_{0x} + v_{0T} - \kappa_2 u_{0x} - Ev_0 + D_x. \end{aligned} \tag{B11}$$

Using the same arguments as described above for the upper layer, we obtain the following solvability condition:

$$\int_{-\infty}^{\infty}(c_2^{(1)}v_{0x} - v_{0T} - u_{0x} - v_0 + D_x)v_0\,d\theta_2 = 0, \tag{B12}$$

which yields the evolution equation for the solitary-wave amplitude a_2,

$$\begin{aligned} \frac{da_2}{dT}(T) = -2\kappa_2 a_1 w_1 \int_{-\infty}^{\infty}\mathrm{sech}^2(\theta_2)\,\mathrm{sech}^2\left(\frac{w^1}{w_2}\theta_2 + w_1\Delta\Phi\right)\tanh\left(\frac{w_1}{w_2}\theta_2 + w_1\Delta\Phi\right)d\theta_2 - \frac{4}{3}Ea_2 \\ + w_2\int_{-\infty}^{\infty}\mathrm{sech}^2(\theta_2)D_{\theta_2}\left(\frac{\theta_2}{w_2} + \Phi_2\right)d\theta_2. \end{aligned} \tag{B13}$$

The amplitude equations (B10) and (B13) contain the leading-order energy balance, as can be seen by inserting u_0 and v_0 into the full system (B1), multiplying the first equation by u_0 and second one by v_0, and integrating over the whole spatial domain.

At this order the first-order speed corrections $c_i^{(1)}$ remain undetermined and the phase equation is just

$$\frac{d\Delta\Phi}{dt} = \Delta_2 - \Delta_1 - 2a_2 + 2\mu a_1. \tag{B14}$$

To determine $c_i^{(1)}$ it is first necessary to obtain u_1 and v_1, and then apply a solvability condition to the linear equations for u_2 and v_2 analogous to (B7) and (B11), respectively. We shall not give details as the procedure is analogous to that described by Grimshaw and Mitsudera (1993) (see also Grimshaw et al. 1995). However, it is pertinent to note first that the solutions for u_1 and v_1 contain terms $U_1^{\pm} = u_1(\pm\infty)$ and $V_1^{\pm} = v_1(\pm\infty)$, respectively, indicative of radiative tails. Indeed it is readily shown from (B7) that

$$U^+ - U^- = -\frac{a_{1T}}{2\mu a_1 w_1}, \tag{B15}$$

and analogously from (B11),

$$V^+ - V^- = -\frac{a_{2T}}{2a_2 w_2} - \frac{E}{w_2}. \tag{B16}$$

Because the radiative tails are essentially linear waves, they propagate ahead of (behind) the solitary wave for the u component according as $\lambda > 0$ (<0), and ahead of the solitary wave for the v component, which can be easily seen by moving into a frame of reference in which the solitary wave is stationary. Thus we set $U^{\mp} = 0$ according to $\lambda > 0$ (<0) and $V^- = 0$. The full expression for $c_i^{(1)}$ is quite complicated and described by a further pair of differential equations. Here, however, we shall follow standard practice and use approximate expressions for $c_i^{(1)}$ valid on the intermediate timescale $T \ll 1$ or $t \ll \epsilon^{-1}$. Thus,

$$c_1^{(1)} = \mu(U^+ - U^-) + \frac{1}{2a_1 w_1}\int_{-\infty}^{\infty} [\tanh(\theta_1) + \theta_1 \operatorname{sech}^2(\theta_1)]\kappa_1 v_{0x}\, d\theta_1, \tag{B17}$$

and

$$c_2^{(1)} = (V^+ + V^-) + \frac{1}{2a_2 w_2}\int_{-\infty}^{\infty} [\tanh(\theta_2) + \theta_2 \operatorname{sech}^2(\theta_2)](\kappa_2 u_{0x} - D_x)\, d\theta_2, \tag{B18}$$

Let us next summarize the results for the asymptotic equations for the amplitudes and the phases [(B10), (B13), (B14), (B17), and (B18)] while restoring the original version of the parameters κ_1, κ_2, and F. Thus we obtain the set of ordinary differential equations:

$$\frac{da_1}{dt} = -2\kappa_1 a_2 w_2 \int_{-\infty}^{\infty} \operatorname{sech}^2(\psi)\operatorname{sech}^2\left(\frac{w^2}{w_1}\psi - w_2\Delta\Phi\right)\tanh\left(\frac{w_2}{w_1}\psi - w_2\Delta\Phi\right) d\psi,$$

$$\frac{da_2}{dt} = -2\kappa_2 a_1 w_1 \int_{-\infty}^{\infty} \operatorname{sech}^2(\psi)\operatorname{sech}^2\left(\frac{w^1}{w_2}\psi + w_1\Delta\Phi\right)\tanh\left(\frac{w_1}{w_2}\psi + w_1\Delta\Phi\right) d\psi - \frac{4}{3}Ea_2$$
$$+ w_2\int_{-\infty}^{\infty} \operatorname{sech}^2(w_2\psi) D_{\psi}(\psi + \Phi_2)\, d\psi,$$

$$\frac{d\Phi_1}{dt} = \Delta_1 - 2\mu a_1 - \kappa_1\frac{\mu}{\lambda}\frac{w_2^3}{w_1^3}\int_{-\infty}^{\infty} [\tanh(\psi) + \psi\operatorname{sech}^2(\psi) - \operatorname{sgn}(\lambda)\tanh^2(\psi)]\operatorname{sech}^2\left(\frac{w_2}{w_1}\psi - w_2\Delta\Phi\right)$$
$$\times \tanh\left(\frac{w^2}{w_1}\psi - w_2\Delta\Phi\right) d\psi,$$

$$\frac{d\Phi_2}{dt} = \Delta_2 - 2a_2 - \kappa_2 \frac{\lambda}{\mu} \frac{w_1^3}{w_2^3} \int_{-\infty}^{\infty} [\tanh(\psi) + \psi \operatorname{sech}^2(\psi) - \tanh^2(\psi)] \operatorname{sech}^2\left(\frac{w_1}{w_2}\psi + w_1\Delta\Phi\right) \times \tanh\left(\frac{w^1}{w_2}\psi + w_1\Delta\Phi\right) d\psi + \frac{1}{2a_2} \int_{-\infty}^{\infty} [\tanh(w_2\psi) + w_2\psi \operatorname{sech}^2(w_2\psi) - \tanh^2(w_2\psi)] D_\psi(\psi + \Phi_2)\, d\psi - \frac{E}{3w_2}. \quad \text{(B19)}$$

REFERENCES

Arakawa, A., 1966: Computational design for long term numerical integration of the equations of fluid motion: Two-dimensional incompressible flow. Part I. *J. Comput. Phys,* **1,** 119–143.

Bartello, P., 1995: Geostrophic adjustment and inverse cascades in rotating stratified turbulence. *J. Atmos. Sci.,* **52,** 4410–4428.

——, O. Metais, and J. Lesieur, 1996: Geostrophic versus wave eddy viscosities in atmospheric models. *J. Atmos. Sci.,* **53,** 564–571.

Bokhove, O., and T. Shepherd, 1996: On Hamiltonian balanced dynamics and the slowest invariant manifold. *J. Atmos. Sci.,* **53,** 276–297.

Cehelsky, P., and K. K. Tung, 1985: Theories of multiple equilibria and weather regimes—A critical reexamination. Part 2: Baroclinic two-layer models. *J. Atmos. Sci.,* **42,** 2804–2819.

Charney, J., 1947: The dynamics of long waves in a baroclinic westerly current. *J. Meteor.,* **4,** 135–163.

——, and J. DeVore, 1979: Multiple flow equilibria in the atmosphere and blocking. *J. Atmos. Sci.,* **36,** 1205–1216.

Christensen, C. W., and A. Wiin-Nielsen, 1996: Blocking as a wave–wave interaction. *Tellus,* **48,** 254–271.

Craik, A. D. D., 1985: *Wave Interactions in Fluid Flows.* Cambridge University Press, 322 pp.

Dole, R. M., 1982: Persistent anomalies of the extratropical Northern Hemisphere wintertime circulation. Ph.D. thesis, Massachusetts Institute of Technology.

——, 1983: Persistent anomalies of the extratropical Northern Hemisphere wintertime circulation. *Large-Scale Dynamical Processes in the Atmosphere,* B. J. Hoskins and R. P. Pearce, Eds., Academic Press, 95–109.

——, 1986: The life-cycles of persistent anomalies and blocking over the North Pacific. *Advances in Geophysics,* Vol. 29, Academic Press, 31–70.

Eady, E. T., 1949: Long waves and cyclonic waves. *Tellus,* **1,** 33–52.

Egger, J., W. Metz, and G. Mueller, 1986: Forcing of planetary-scale blocking anticyclones by synoptic-scale eddies. *Advances in Geophysics,* Vol. 29, Academic Press, 183–197.

Ek, N. R., and G. E. Swaters, 1994: Geostrophic scatter diagrams and the application of quasigeostrophic free-mode theory to a northeast Pacific blocking episode. *J. Atmos. Sci.,* **51,** 563–581.

Frederiksen, J., 1992: Towards a unified instability theory of large-scale atmospheric disturbances. *Trends Atmos. Sci.,* **1,** 239–261.

——, 1997: Adjoint sensitivity and finite-time normal mode disturbances during blocking. *J. Atmos. Sci.,* **54,** 1144–1165.

——, and R. Bell, 1990: North Atlantic blocking during January 1979: Linear Theory. *Quart. J. Roy. Meteor. Soc.,* **116,** 1289–1313.

Gierling, J., 1994: Wechselwirkung Strahlstrominduzierter Rossby-Wellen in der Erdatmosphäre. Ph.D. thesis, Universität Düsseldorf, 141 pp.

Gottwald, G., 1998: Nonlinear waves and pattern formation in the atmosphere. Ph.D. thesis, Monash University, 102 pp.

Grimshaw, R., and H. Mitsudera, 1993: Slowly varying solitary wave solutions of the perturbed Korteweg-de Vries equation revisited. *Stud. Appl. Math.,* **90,** 75–86.

——, and B. Malomed, 1994: A new type of gap soliton in a coupled Korteweg-De Vries wave system. *Phys. Rev. Lett.,* **72,** 324–335.

——, E. Pelinovsky, and X. Tian, 1995: Interaction of a solitary wave with an external force. *Physica D,* **77,** 405–433.

Haines, K., and J. Marshall, 1987: Eddy-forced coherent structures as a prototype of atmospheric blocking. *Quart. J. Roy. Meteor. Soc.,* **113,** 681–704.

——, and P. Malanotte-Rizzoli, 1991: Isolated anomalies in westerly jet-streams: A unified approach. *J. Atmos. Sci.,* **48,** 510–526.

Han, T. Y., J. C. S. Meng, and G. E. Innis, 1983: An open boundary condition for incompressible stratified fluid. *J. Comput. Phys.,* **49,** 276–297.

Hansen, A., and T. C. Chen, 1982: A spectral energetics analysis of atmospheric blocking. *Mon. Wea. Rev.,* **110,** 1146–1159.

——, and A. Sutera, 1984: A comparison of the spectral energy and enstrophy budgets of blocking versus non-blocking periods. *Tellus,* **36,** 52–63.

Helfrich, K. R., and J. Pedlosky, 1993: Time-dependent isolated anomalies in zonal flows. *J. Fluid Mech,* **251,** 377–409.

——, and ——, 1995: Large-amplitude coherent anomalies in baroclinic zonal flows. *J. Atmos. Sci.,* **52,** 1615–1629.

Holland, W. R., 1978: The role of mesoscale eddies in the general circulation of the ocean—Numerical experiments using a wind-driven quasigeostrophic model. *J. Phys. Oceanogr.,* **8,** 363–392.

Johnson, R., 1973: On an asymptotic solution of the Korteweg-de Vries equation with slowly varying coefficients. *J. Fluid Mech.,* **86,** 415–446.

Kalnay, E., and K. C. Mo, 1986: Mechanistic experiments to determine the origin of short-scale Southern Hemisphere stationary Rossby waves. *Advances in Geophysics,* Vol. 29, Academic Press, 415–442.

Karpman, V., and E. Maslov, 1978: Structure of tails produced under the action of perturbations on solitons. *Sov. Phys. JETP,* **48,** 252–259.

Kaup, D., and A. Newell, 1978: Solitons as particles, oscillators, and in slowly changing media: A singular perturbation theory. *Proc. Roy. Soc. London,* **361A**, 412–446.

Legras, B., and M. Ghil, 1985: Persistent anomalies, blocking and variation in atmospheric predictability. *J. Atmos. Sci.,* **42,** 433–471.

Linden, P. F., B. M. Boubnov, and S. B. Dalziel, 1995: Source-sink turbulence in a rotating stratified fluid. *J. Fluid Mech.,* **298,** 81–203.

Lindzen, R. S., 1986: Stationary planetary waves, blocking, and interannual variability. *Advances in Geophysics,* Vol. 29, Academic Press, 251–276.

Lorenz, E., 1980: Attractor sets and quasigeostrophic equilibrium. *J. Atmos. Sci.,* **37,** 1685–1699.

Lupo, A., and P. Smith, 1995: Planetary and synoptic-scale interactions during the life cycle of a midlatitude blocking anticyclone over the North Atlantic. *Tellus,* **47A,** 575–596.

Malguzzi, P., and P. Malanotte-Rizzoli, 1984: Nonlinear stationary Rossby waves on nonuniform zonal winds and atmospheric blocking Part I: The analytical theory. *J. Atmos. Sci.,* **41,** 2620–2628.

——, and ——, 1985: Coherent structures in a baroclinic atmosphere.

Part II: A truncated model approach. *J. Atmos. Sci.,* **42,** 2463–2477.

Malomed, B., R. Grimshaw, and X. Tian, 1994: Gap solitons in a coupled Korteweg-De Vries system. *Structure and Dynamics of Nonlinear Waves in Fluids,* K. Kirchgässner and A. Mielke, Eds., World Scientific.

Metais, O., P. Bartello, E. Garnier, and J. Lesieur, 1996: Inverse cascade in stratified rotating turbulence. *Dyn. Atmos. Oceans,* **23,** 193–203.

Mitsudera, H., 1994: Eady solitary waves: A theory of type B cyclogenesis. *J. Atmos. Sci.,* **51,** 3137–3154.

Mullen, S. L., 1987: Transient eddy forcing and blocking flows. *J. Atmos. Sci.,* **44,** 3–22.

Naulin, V., 1995: Nichtlinearer transport in Ebenen Driftwellenmodellen. Ph.D. thesis, Universität Düsseldorf, 119 pp.

——, K. H. Spatschek, S. Musher, and L. I. Piterberg, 1995: Properties of a two-nonlinearity mode. *Phys. Plasmas 2,* **48,** 2640–2652.

Nezlin, P., 1994: Rossby solitary vortices on giant planets and in the laboratory. *Chaos,* **4,** 187–202.

Oort, A., and E. Rasmusson, 1971: Atmospheric circulation statistics. NOAA Prof. Paper 5.

Patoine, A., and T. Warn, 1982: The interaction of long, quasi-stationary baroclinic waves with topography. *J. Atmos. Sci.,* **39,** 1018–1025.

Pedlosky, J., 1987: *Geophysical Fluid Dynamics.* 2d ed. Springer-Verlag, 710 pp.

Tang, Y., and R. Grimshaw, 1996: Radiation boundary conditions in barotropic coastal ocean numerical models. *J. Comput. Phys.,* **123,** 96–110.

Tung, K. K., and A. J. Rosenthal, 1985: Theories of multiple equilibria—A Critical Reexamination. Part I: Barotropic models. *J. Atmos. Sci.,* **42,** 2804–2819.

Valcke, S., and J. Verron, 1996: Cyclone–anticyclone asymmetry in the merging process. *Dyn. Atmos. Oceans,* **24,** 227–236.

Warn, T., and B. Brasnett, 1983: The amplification and capture of atmospheric solitons by topography: A theory of onset of regional blocking. *J. Atmos. Sci.,* **40,** 28–40.

——, and R. Menard, 1986: Nonlinear balance and gravity-inertial wave saturation in a simple atmospheric model. *Tellus,* **38,** 285–294.

Yano, J., and H. Mukougawa, 1992: The attractor dimension of a quasi-geostrophic two layer system. *Geophys. Astrophys. Fluid Dyn.,* **65,** 77–91.